General Disclaimer

One or more of the Following Statements may affect this Document

- This document has been reproduced from the best copy furnished by the organizational source. It is being released in the interest of making available as much information as possible.

- This document may contain data, which exceeds the sheet parameters. It was furnished in this condition by the organizational source and is the best copy available.

- This document may contain tone-on-tone or color graphs, charts and/or pictures, which have been reproduced in black and white.

- This document is paginated as submitted by the original source.

- Portions of this document are not fully legible due to the historical nature of some of the material. However, it is the best reproduction available from the original submission.

NASA CONTRACTOR REPORT 166565 - Pt - 3

Solution of Three-Dimensional Time-Dependent Viscous Flows
Part 3: Application to Turbulent and Unsteady Flows

Bernard C. Weinberg
Henry McDonald

CONTRACT NAS2- 10016
September 1982

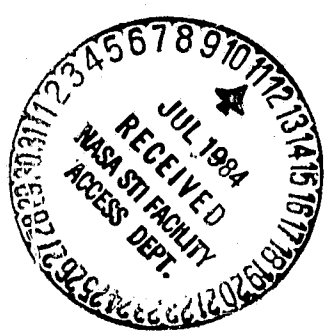

NASA

NASA CONTRACTOR REPORT 166565

Solution of Three-Dimensional Time-Dependent Viscous Flows
Part 3: Application to Turbulent and Unsteady Flows

Bernard C. Weinberg
Henry McDonald
Scientific Research Associates, Inc.
Glastonbury, Connecticut

Prepared for
Ames Research Center
under Contract NAS2-10016

National Aeronautics and
Space Administration

Ames Research Center
Moffett Field, California 94035

TABLE OF CONTENTS

TABLE OF CONTENTS (Cont.)

SUMMARY

The flow over a helicopter rotor is an important example of three-dimensional time-dependent viscous flow. The boundary layers that develop on the rotor blades play a significant role in that they set loss levels and control retreating blade stall. Consequently, there is considerable interest in developing a numerical scheme for solving the time-dependent, three-dimensional compressible viscous flow equations in order to predict such flow fields, and which can be used as an aid in the design of helicopter rotors.

In order to further investigate the numerical procedure, we have exercised the computer code that was developed under a previous phase of the current research program to solve an approximate form of the three-dimensional unsteady Navier-Stokes equations employing a Linearized Block Implicit technique in conjunction with a QR operator scheme. Results of calculations are presented for several two-dimensional boundary layer flows including steady turbulent and unsteady laminar cases.

A comparison of fourth order and second order solutions indicate that increased accuracy can be obtained without any significant increase in cost (run time). The results of the computations also indicate that the computer code can be applied to more complex flows such as those encountered on rotating airfoils. Finally, th geometry of a symmetric NACA four digit airfoil is considered and the appropriate geometrical properties are computed.

INTRODUCTION

The behavior of boundary layers on wings and bodies has long been of interest to aerodynamicists. In both steady and unsteady flows, the boundary layers are known to govern a major portion of the losses and to significantly influence the vehicle lift and moment coefficients. When the flow is steady, boundary layer prediction schemes based on numerical solution to the governing partial differential equations of motion have reached a high level of sophistication and predictive accuracy, even in three space dimensions. In unsteady flows, such as are commonly encountered in rotary winged aircraft, some progress has been made in two space dimensions but little to date has appeared on unsteady three-dimensional boundary layers.

Two particular problems arise with time-dependent three-dimensional boundary layers relative to the steady case. The first of these is the rather obvious one of time integration with its added requirements of transient accuracy coupled with an increase in the computational labor. The second of these is the so-called negative cross flow problem, which to some extent has troubled the steady boundary layer prediction schemes. Kendall, et al (Ref. 1) discuss the negative cross flow problem for steady three-dimensional boundary layers in a very illuminating fashion. This particular problem arises when the spanwise component of velocity changes sign and will be discussed in detail subsequently. Because of the interest by external aerodynamicists in swept wing boundary layers where the negative cross flow problem (in this case flow from tip to root) is not usually encountered, the negative cross flow problem has not received a great deal of attention to date. However, in transient flows, particularly those encountered on rotor blades in forward flight, negative cross flows are frequently encountered. For instance, the advancing rotor blade has cross flows of one sign during the first ninety degrees of rotation and these can change sign over part of the blade during the second ninety degrees.

Thus to be of practical value, time-dependent three-dimensional boundary layer prediction schemes require high computational efficiency and transient accuracy coupled to the ability to treat arbitrary cross flow profiles.

In this report we describe the development of a computer code for the efficient solution of three-dimensional time-dependent viscous flows on fixed and rotary aircraft. The Linearized Block Implicit (LBI) technique of Briley and McDonald (Ref. 2) in coordination with a tridiagonal QR operator scheme (Ref. 3) is employed to solve the reduced turbulent Navier-Stokes equations which are derived for nonorthogonal

coordinates in generalized tensor form. The rationale for the choice of this approach is discussed in detail in Ref. 3 and 4.

The basic assumptions made in the derivation of these equations are that the pressure does not vary normal to the shear layer and that in the energy equation the square of the normal velocity is neglected with respect to the other velocity components (To = constant). The latter assumption is included only for computational simplification purposes and is not essential in the analysis. For turbulent flows, a two-layer mixing length model is employed and its formulation in generalized tensor notation is given. A novel method is employed for solving the continuity equation in conjunction with the reduced Navier-Stokes equations. The continuity equation is split by employing the Douglas-Gunn procedure to obtain a consistent approximation to the full equation which is then solved as an integral. Results of several boundary layer calculations are presented and comparisons with experimental data and other reported computations are made.

LIST OF SYMBOLS

a, b, c, d	coefficients of differential equation
a_{ij}^{n}	coefficient of differential operator
B	Binormal vector
C_f	skin friction coefficient
$\mathcal{D}$	nonlinear three-dimensional differential operator
$\vec{e}_i$	covariant basis vector
f_j, $f(x)$	right-hand side of differential equation
g_{ij}, g^{ij}	components of metric tensor
H	shape factor
h	step size
h_1, h_2	scale factors
J	Jacobian
K	curvature
K_g	geodesic curvature
K_n	normal curvature
ℓ	mixing length
$L(u)$	linear differential operator
$\mathcal{L}_i$	linear three-dimensional differential operator
L_i	product operator $\vec{Q}_i \mathcal{L}_i$.
M^n	difference between $\mathcal{D}^n$ and $\mathcal{L}^n$
$\vec{N}$	normal vector
P	pressure
Q	tridiagonal difference operator
q^-, q^c, q^+	components of Q
$\vec{q}$	velocity vector
R	tridiagonal difference operator

r^-, r^c, r^+	components of R
R_e	Reynolds number
R_{c_j}	cell Reynolds number
S^n	source term
t	time
T	static temperature
T_o	stagnation temperature
u^i	contravariant velocity component
u, v, w	physical velocity component
x^i	coordinate direction in i direction

GREEK SYMBOLS

β	factor for centering time step
γ	ratio of specific heats
Γ^k_{ij}	Christoffel symbol
δ	boundary layer thickness
δ^*	displacement thickness
δ^i_j	Kronecker delta function
Δ	velocity divergence
Δt	time step
Δx_i	step size in i direction
θ	momentum thickness
ε^{jk}	strain tensor
η	boundary layer coordinate
λ	viscous stability parameter
μ	molecular viscosity
ρ	density

σ^{ik}	stress tensor
Φ	dissipation function
ϕ	vector of unknowns in LBI scheme
ψ	source term in LBI scheme
τ_w	wall shear
ω	frequency of oscillation

SUBSCRIPTS

e	edge
p	physical
∞	free stream

SUPERSCRIPTS

n	time level
*, **, ***	intermediate time level in ADI procedure

ANALYSIS

Background

Three-dimensional boundary layers occur on the wings and fuselages of both fixed and rotary wing aircraft. In both types of vehicles, the boundary layers are important in setting loss levels and determining useful operating ranges. As is well known, boundary layers are sensitive to pressure gradients. In time-dependent flow the temporal acceleration terms appear in the momentum equation in a form very similar to the conventional imposed pressure gradient and so for qualitative evaluation purposes can be regarded as "pseudo" or "auxiliary" pressure gradients. Viewed in this manner, the temporal acceleration terms can be seen to influence quantities of practical importance such as skin friction, displacement thickness and the onset of separation. At the range of frequencies typically encountered in rotary wing aircraft aerodynamic problems, it is clear, for instance, from the extensive review of McCroskey (Ref. 5), that very significant transient boundary layer effects can be observed.

In examining the flow problems of practical interest such as loss levels or the onset of separation it is evident that all three space dimensions must be considered. In conventional aircraft, the sweep effect is of interest and inherently three-dimensional. In rotary wing aircraft, in forward flight clearly very substantial transient changes occur in what might be termed the local sweep angle. However, generally speaking, the boundary layers remain thin unless catastrophic flow separation occurs or the flow at the wing or rotor tip is considered.

Conventional boundary layer integration schemes have developed by forward marching the streamwise velocity u in the streamwise x direction and simultaneously marching out along the span in the z positive direction. In general, the spanwise marching scheme does not normally encounter negative w, i.e., spanwise inflow. This is very fortunate because it is difficult, indeed it could be argued impossible, to structure a physically satisfactory unconditionally stable noniterative scheme which permits forward marching in the spanwise direction with a negative w cross flow. At least intuitively the problem of negative cross flow implies information being transferred upstream against the spanwise marching direction. Conventional stability analyses confirm the inability to forward march into regions of significant negative w. From experience with attempts to march the two-dimensional boundary layer equations into a region of separated flow and its obvious relationship to the negative cross

flow problem, it is not surprising that spanwise marching into a negative cross flow region is not accomplished without special treatment. Recently, conventional boundary layer developers have been turning to performing an implicit spanwise construction to remove the restriction of only positive cross flows (Kendall, et al, Ref. 1). Lin and Rubin (Ref. 6) in their predictor-corrector boundary region solutions for flow over a yawed cone at moderate incidence have also shown that retaining diffusion in the spanwise direction not only eliminates the problems associated with negative cross flows, but improves upon the solutions obtained by standard three-dimensional boundary layer techniques. Furthermore, boundary conditions applied at the tip can influence the flow inboard, if required by the physics of the flow.

For these reasons, the implicit spanwise construction has been a feature of the three-dimensional duct flow analysis of Briley (Ref. 7) and McDonald and Briley (Ref. 8). As a consequence of these observations and the need to remove the negative cross flow restriction, a spanwise implicit formulation seems mandatory for rotary wing applications and at least desirable for fixed wing applications, expecially as it can be had for a very modest increase in code computational labor. Based on the experience in Refs. 7 and 8, the spanwise implicit sweep would only result in a moderate increase in computational effort relative to the explicit spanwise marching approach. The extension of the conventional three-dimesional boundary layer equations to allow spanwise diffusion is easily accomplished, and in view of the improved physical representation which thus follows, it is recommended and has been implemented in this effort.

As a matter of course, it has been assumed that normal to the wall an implicit formulation would be structured. In recent years for boundary layer type problems there has been little dispute as to the efficiency gains to be had from an implicit formulation normal to the wall (Ref. 9). However, in the streamwise direction for steady 2-D flow, the equations are normally forward marched and the implicit stability obtained entirely from being implicit in the normal to the wall direction. In time-dependent flows a similar structure is to be had so that at each time level one streamwise (explicit) forward marching sweep could be made with two implicit sweeps in the spanwise and normal directions to give the desired unconditional stability. As mentioned earlier, the explicit sweep would probably require less computational effort by about 20% than an implicit streamwise sweep and of course less storage. However, since the solution is being time marched the opportunity to take a streamwise implicit sweep at roughly the same cost as the explicit sweep

does arise. If one does perform a streamwise explicit sweep, then the linearization of nonlinear terms is performed about the known spatial marching level. If an implicit streamwise structure is adopted, then full time linearization can be utilized. That is the linearization of the nonlinear terms is performed about the known time level. As is pointed out in Ref. 8, it is easier to obtain a consistent high order accurate spatial-temporal linearization by marching in time than in space (in time the marching derivatives have the form u_i whereas in space they are nonlinear and have the form $u_i u_j$). Further, by structuring implicitly in the space marching direction, small regions of axial reverse flow would be permitted. As a result of the combined benefits of consistent high order linearizations and the inclusion of small separated zones, a streamwise implicit structure is advocated and has been employed in this effort.

Since a full 3-D spatial integration is carried out at each time step of a transient calculation, spatial accuracy plays a very important role in the overall efficiency of the numerical method. By choosing a spatial scheme of sufficient accuracy, one can expect to reduce the total number of grid points to an acceptable level. However, for the chosen scheme one must account not only for the spatial discretization errors but those introduced as a result of the linearization procedure. In order to get the most out of a given spatial difference formula, the errors incurred in representing nonlinear terms by linear combinations of terms should be less than or equal to the spatial discretization errors. If the linearization introduces a greater error than the spatial differencing, then either a coarser spatial mesh could be used, or iteration, or some form of linearization improvement is called for. Iteration across a time step is not recommended since this only reduces the linearization error and computationally costs as much as a complete time step. Cutting back the time step would be prefereable to iterating to preserve the linearization error at some acceptable level, since cutting back on the time step would improve both the transient error and the linearization error. This point is clearly demonstrated in Ref. 3. To obtain a linearization, which introduces errors of at most the same as the spatial difference formulae, a Taylor series expansion about the known time level can be performed. This process clearly demands a formal block, i.e., coupled, treatment of the system of equations. For instance, in the streamwise momentum equation a typical term is linearized:

$$(uw)^{n+1} = u^{n+1}w^n + u^n w^{n+1} - u^n w^n + O(\Delta t^2)$$

and clearly one cannot lag w^{n+1} at the old time level n without introducing a first-order time error in order to get an uncoupled system, i.e., w^{n+1} not appearing in the streamwise momentum equation. Thus, formal linearization and consideration of the resulting errors indicate the coupled system ought to be treated from the accuracy point of view. This is further reinforced when it is realized that block, i.e., coupled, systems are not computationally expensive (in a relative sense).

Additionally, a second type of approximation arises unconnected with linearization but arising from basic coupling terms in the original equations and if indeed some terms in an equation are time lagged in order to uncouple the equation system and these terms are of equal importance to the terms retained, then again an iterative updating is called for in order to achieve stability, accuracy and consistency. This could be termed ad hoc equation uncoupling. Blottner (Ref. 9) has shown that many iterations around the ad hoc uncoupled set (> 10) are sometimes required in order to achieve an overall solution accuracy commensurate with the local difference molecule accuracy.

The linearization technique discussed above is described in Ref. 8, together with its application to block coupled splitting schemes. Schemes of this general type are here referred to as "split linearized block implicit" or split LBI schemes, and are reviewed in detail by Briley and McDonald (Ref. 2).

As a general observation, care is required to obtain acceptable transient accuracy for long time integration with conventional finite difference schemes. A Crank-Nicolson centered time-implicit scheme for instance, although second order in time, shows quite a dispersion problem (relative to other schemes) on the simple pure convection problem. However, the problem of transient accuracy is significantly reduced in the typical boundary layer problem since the time dependency is continuously input through boundary conditions and the concern is with relatively "short" time integrations. The computational problem is more of what the phase lag of the wall shear is, relative to the prescribed free stream disturbance, than concern over the convection velocity of a wave in a shear after a long propagation time. The interest is in forced oscillations with a minimum scale of the boundary layer thickness over a few cycles of the motion, just enough to obtain repetition cyclically. It is, therefore, expected that a significant dispersion problem will not arise with a conventional implicit scheme.

The governing equations that are considered here are the Navier-Stokes equations, continuity, energy and the equation of state which are written in generalized tensor form for a body oriented coordinate system (boundary layer coordinates). In

accordance with the boundary layer assumptions, the normal momentum equation is eliminated and the pressure is specified throughout the viscous layer in its stead. For the energy equation, constant stagnation temperature T_o is assumed. This assumption is a good approximation for the flow fields considered, and is thus included here only for purposes of simplification. In the analysis that follows, the full energy equation could equally well have been used. Employing the equation of state which relates the pressure p to the velocity components u and w by an algebraic equation, the problem can be reduced to one involving only the three velocity components, u, w and v and three equations, the streamwise and spanwise momentum equations and the continuity equation. Hence, we consider a block-three system rather than a block-four system which leads to a significant reduction in computer time. If the full energy equation were to be considered, a block-four system would result due to the inclusion of the temperature as an additional unknown.

Coordinate System

Since the goal of this effort is to solve for the flow over airfoils an understanding of the type of geometries to be considered is essential to guide the choice of the coordinate system and the structure of the computer code. The coordinate system is not only dependent upon the geometry of the airfoil, but also upon the approximations that are made to the governing Navier-Stokes equations. As in boundary layer theory, we also assume that in the approximate form of the Navier-Stokes equations the pressure is constant normal to the shear layer. Inherent in the assumptions is that the shear layer is thin. As pointed out by Howarth (Ref. 10) the boundary layer assumptions lead to the conditions that one coordinate direction must be normal to the body surface (this being straight) while the other coordinate directions must lie on the body surface. These conditions uncouple the metric data on the surface from that in the normal direction. Hence, the metric data for the surface coordinates are functions of the surface coordinates alone, while the metric data for the normal coordinate direction are functions of that coordinate alone. The choice of the surface coordinates is rather arbitrary and is based on considerations such as the ease of construction or the grid distribution on the wing surface.

In the numerical solution of the flow over an airfoil there are many advantages to be gained by the judicious choice of coordinates. The most obvious advantage is that the physical boundaries of a flow region can be represented by coordinate surfaces. This removes the need for fractional cells in general; hence, the complications and loss of accuracy associated with a boundary interpolation are removed.

Another advantage is that a uniform numerical method can be used. The solution can then be performed with a fixed number of cells in any given direction and with a uniform mesh spacing. For a rectangular plan form wing a Cartesian coordinate system would be adequate. However, for more general plan forms such as a swept wing a nonorthogonal grid which conforms with the boundaries is preferred since it covers the entire airfoil while a Cartesian grid would not.

Another consideration is the selection of a coordinate grid distribution; the major objective being the resolution of large solution gradients. The approach taken here is to construct coordinate transformations that contain distributions for physical mesh points. In this context, the uniform mesh of computational space is simply mapped into a suitably distributed mesh in physical space. When the transformation contains the mesh point distribution, there is no need to construct the apparatus for the discrete approximation of derivatives on a nonuniform mesh. This results in a savings in both computer logic and storage.

Hence, in this work a coordinate system is chosen that conforms with the boundaries of the physical domain, i.e., the wing surface which in general will be nonorthogonal. In addition, provisions are made for analytical grid transformations (Ref. 11) in each coordinate direction, in order to suitably distribute grid points in regions of large gradients.

In view of the type of geometries to be considered and the assumptions made to obtain the approximate form of the Navier-Stokes equations, a specialized nonorthogonal coordinate system is advocated where the metric tensor which has four independent components is given by

$$g_{ij} = \begin{bmatrix} g_{11} & g_{12} & 0 \\ g_{12} & g_{22} & 0 \\ 0 & 0 & g_{33} \end{bmatrix}$$

The subscripts 1 and 2 refer to the directions on the surface of the body while subscript 3 refers to the direction normal to the body. Since the metric data in the coordinate directions on the airfoil surface are not functions of the normal direction, the metric data in a 1 - 2 surface above the body are evaluated on the body surface (Ref. 10). Furthermore, due to the use of nonorthogonal coordinates

it becomes advantageous to derive the equations in general nonorthogonal coordinates employing generalized tensors. Details of the generalized tensor notation can be found in Refs. 12, 13, and 4.

An important feature of the analysis to follow is that the governing equations which are derived, under the prescribed assumptions, are invariant for any coordinate system or any grid transformation (although, of course, the physical approximations are coordinate dependent). The grid transformations are absorbed into the geometrical coefficients, leaving the equations unaltered in form. This feature allows for the construction of the geometric data to be contained in one subroutine with the definition of the metric data and their derivatives as input.

Other forms of the governing equations for nonorthogonal coordinates which do not rely on generalized tensor notation were considered, i.e., such as the steady three-dimensional boundary layer equations as given by Cebeci (Ref.14). Since in that set of equations the only viscous terms retained are these in the normal direction, any nonorthogonal effects are introduced solely through the convective terms. This is a direct consequence of the assumptions which decouple the normal coordinate from the surface coordinates. In those equations, the geometric terms that explicitly appear are the metrics, h_1 and h_2, the geodesic curvatures k_{g_1} and k_{g_2}, the angle between the surface coordinate lines and an additional nonorthogonal curvature term. In contrast to Cebeci's equations, the set of equations considered here, the approximate form of the Navier-Stokes equations, allow for all the viscous terms to be retained. A description of these terms without generalized tensor notation would be cumbersome. Hence, the generalized tensor approach was chosen.

In Appendix B the geometric properties of a surface in three dimensions are discussed and where appropriate, the generalized tensor equivalents are given. In addition, a symmetric (uncambered) NACA four-digit airfoil is considered and the pertinent geometric coefficients are presented.

Governing Equations

In view of the ultimate goal of this program, to solve an approximate form of the unsteady three-dimensional Navier-Stokes equations on airfoil shapes, the governing equations are derived in general nonorthogonal coordinates and are given in generalized tensor notation.

In the following derivation the governing equations are nondimensionalized as follows, x^i with respect to the characteristic length L, the velocity with respect to U_∞, density, pressure and temperature with respect to ρ_∞, $\rho_\infty U_\infty^2$ and U_∞^2/c_p respectively and time with respect to L/U_∞. Viscosity is nondimensionalized with respect to μ_∞.

Continuity Equation

Consider the continuity equation wirtten in vector form so that it is independent of coordinate system, i.e.,

$$\frac{\partial \rho}{\partial t} + \nabla \cdot \rho \vec{q} = 0 \tag{1}$$

where ρ is the density and $\vec{q}$ is the velocity vector, which can be written in a covariant basis as

$$\vec{q} = u^i \vec{e}_i \tag{2}$$

where u^i is the i-th contravariant velocity component and $\vec{e}_i$ is the covariant basis vector in the x^i direction. The velocity vector could have been expressed in a number of different forms, each with its own attribute. Here for the moment the velocity vector is expressed in a covariant basis, for simplicity. Subsequently, the velocity vector will be transformed into its physical components for the numerical solution of the governing equations. The reason for this is that the contravariant basis exhibits variation in its components if the coordinates are such that the metric varies. For boundary layer flows, the physical velocity components are roughly aligned with the coordinates and exhibit no variation with the metric per se. As such, it is felt that the actual computations are better performed on the pnysical components.

The divergence of a vector is given by

$$\nabla \cdot \rho \vec{q} = \rho u^k\big|_k = (\rho u^k)_{,k} + \rho u^i \Gamma^k_{ik} = \frac{1}{J}(J \rho u^k)_{,k} \tag{3}$$

where $\rho u^k|_k$ is the covariant derivative, $\rho u^k{}_{,k}$ is the partial derivative in the x^k direction, J is the Jacobian and Γ^k_{ik} is the Christoffel symbol.

In Equation 3 two forms of the divergence are presented, one involving the Christoffel symbol or curvature term directly and the other the Jacobian. The former is perhaps more restrictive since it requires additional smoothness of the geometrical quantities. However, both forms are used depending on which is more convenient for the given application. For the momentum equations the form involving the Christoffel symbols is employed in the evaluation of the explicit (lagged) diffusion terms while for the continuity equation the form involving the Jacobian is used. Thus, the continuity equation can be expressed as

$$\frac{\partial \rho}{\partial t} + \frac{1}{J}(J \rho u^k)_{,k} = 0 \tag{4}$$

Momentum Equations

The momentum equations in vector form can be written as

$$\rho \frac{\mathcal{D}\vec{q}}{\mathcal{D}t} = \rho\left[\frac{\partial \vec{q}}{\partial t} + (\vec{q}\cdot\nabla)\vec{q} \right] = \nabla \cdot \bar{\bar{\sigma}} \tag{5}$$

where $\bar{\bar{\sigma}}$ is the stress tensor.

In generalized tensor notation, Equation 5 becomes

$$\rho\left[\frac{\partial u^i}{\partial t} + u^k u^i\big|_k \right] \vec{e}_i = \sigma^{ik}\big|_k \vec{e}_i \tag{6}$$

The stress tensor is defined as

$$\sigma^{ik} = -\left[p + \frac{2}{3}\frac{\mu}{Re}\Delta\right]\delta^{ik} + \frac{\mu}{Re}\,\epsilon^{ik} \tag{7}$$

where μ is the viscosity, p is the pressure, Δ is the velocity divergence and ϵ^{ik} is the strain tensor, and the Reynolds number, Re, is defined as $\rho_\infty U_\infty L/\mu_\infty$. The strain tensor expressed in terms of velocity components is

$$\epsilon^{ik} = u^i\big|_m g^{mk} + u^k\big|_m\, g^{im} \tag{8}$$

where g^{mk} and g^{mi} are the components of the metric tensor. Employing the fact that $\delta^{kj} = g^{kj}$ and substituting the definition of the strain into the stress tensor, we obtain

$$\sigma^{ik} = -\left(p + \frac{2}{3}\frac{\mu}{Re}\Delta\right) g^{ik} + \frac{\mu}{Re}\, u^i\big|_m g^{mk} + \frac{\mu}{Re}\, u^k\big|_m g^{mi} \tag{9}$$

Substituting Equation 9 into the momentum equation and employing the relationship

$$g^{kj}\big|_k = 0 \tag{10}$$

we obtain for the i-th momentum equation in the $\vec{e}_i$ direction

$$\rho\left[\frac{\partial u^i}{\partial t} + u^k u^i\big|_k\right] = -g^{ik}\left(p + \frac{2}{3}\frac{\mu}{Re}\Delta\right)_{,k} + g^{mk}\left[\frac{\mu}{Re}u^l\big|_m\right]\big|_k + g^{mi}\left[\frac{\mu}{Re}u^k\big|_m\right]\big|_k \tag{11}$$

In Ref. 3 it was pointed out that the QR operator scheme requires that derivatives in any direction operate on only one variable. In the momentum equation this requirement prevents the implicit treatment of certain diffusion terms that arise due to the curvature of the body. Although these terms are often treated explicitly anyway the use of standard finite difference techniques instead of the QR operators would give one the opportunity to treat these terms implicitly, if so desired. This and the use of the quasi-linear form of the governing equations are the only major limitations that arise in the QR operator treatment of the approximate form of the Navier-Stokes equations. In the usual boundary layer approximations, these explicitly treated terms would not appear in the equations since they are of order 0 $(Re^{-1/2})$ or smaller, and should, therefore, be of little consequence. In principle, the quasi-linear and, for instance, the full conservative form of the differential equations, are equivalent. In discrete form, various formulations of the governing equations exhibit different properties (Ref. 15). In the present problem, no distinct disadvantage appears to arise from the required use of a quasi-linear form of the governing equations.

The requirement that derivatives in any direction operate only on one variable would be more restrictive in the treatment of the pressure gradient term in the full Navier-Stokes equations. The linearization of this term introduces derivatives of all the velocity components in a given direction. According to the limitations of the QR operator scheme described above, some of these terms must be treated explicitly. Since an explicit treatment of these terms could reduce the stability bound of the calculation scheme, an alternate procedure should be considered. This would involve the addition of an auxillary equation relating the pressure gradient term to the derivatives of the velocity components and would increase the block size of the system. An assessment of the efficiency of such a procedure has not been carried out and further work in this area would appear to be warranted.

In the discussion that follows, the governing equations are first split into an explicit part and an implicit part in accordance with the QR operator requirements. Thereafter, the resulting equations are cast into "standard form", so that the equations can be appropriately linearized and treated with the LBI technique.

Since mixed partial derivatives are commonly treated explicitly in orthogonal coordinate systems, a similar procedure will be used for generalized nonorthogonal coordinates where the explicit treatment is extended to include mixed second covariant derivatives. All other second covariant derivatives are retained as implicit. Although such a procedure would automatically treat more terms explicitly than one does for orthogonal coordinates, it simplifies the bookkeeping requirements in the

construction of the computer code, and is thus adopted here. Conversely, retaining the covariant derivative as a unit (whether implicit or explicit) could prevent instabilities that may arise due to time splitting. This can occur when two portions of one term should cancel identically, but do not due to their being split between two sweeps.

Diffusion Terms

Consider the term

$$(\mu u^m|_j)|_k \tag{12}$$

If j = k the term is retained as implicit, and if j ≠ k then it is treated explicitly. We will consider the case j ≠ k first. Upon expanding the explicit part of the diffusion term, it becomes

$$(\mu u^i|_j)|_k = \left[\mu(u^i{}_{,j} + u^n \Gamma^i_{jn})\right]_{,k} + \mu\left[u^m{}_{,j} + u^n \Gamma^m_{jn}\right]\Gamma^i_{mn} - \mu\left[u^i{}_{,m} + u^n \Gamma^i_{mn}\right]\Gamma^m_{jk} \tag{13}$$

Note that the first term on the right-hand side of the equation is in conservation form. Although the implicit equations are treated in quasi-linear form, for the purpose of evaluating the explicit terms the most convenient representation is used. The implicit terms, with j = k become (note there is no sum on j)

$$(\mu u^i|_j)_j = \mu(u^i{}_{,j})_{,j} + \left[(\mu u^n)_{,j}\Gamma^i_{jn} + \mu u^n{}_{,j}\Gamma^i_{jn} - \mu u^i{}_{,n}\Gamma^n_{jj}\right] + (\mu S^i{}_{jnj})u^n + T^i_{jj} \tag{14}$$

where

$$S^i{}_{jnj} = \Gamma^m_{jn}\Gamma^i_{mj} - \Gamma^i_{mn}\Gamma^m_{jj} + \Gamma^i_{jn,j} \tag{15}$$

and

$$T^i_{jj} = 2\mu\left[u^m{}_{,j}\Gamma^i_{mj} + u^m{}_{,j}\Gamma^l_{mj}\right] + \mu_{,j}\left[u^m\Gamma^i_{mj} + u^n\Gamma^l_{jn}\right] \tag{16}$$

m = i + 1, n = 5 - 2i and there is no sum on m and n

Since T^i_{jj} involves velocity components and derivatives in directions other than the i-th direction, the term is also treated explicitly.

Hence the total diffusion terms for the i-th momentum equation is given in

quasi-linear form as

$$\sum_{j=1}^{3}\Big\{\Big[c_1^j g^{jj}\mu\Big]u^i_{,jj}+\Big[c^j g^{jj}(\mu_{,j}+2\mu\Gamma^i_{jl})-\sum_{k=1}^{3}c_1^k g^{kk}\mu\Gamma^j_{kk}\Big]u^i{}_{,j}$$
$$+\delta_1^j\Big[\sum_{k=1}^{3}c_1^k g^{kk}\mu_{,k}\Gamma^l_{kl}\Big]u^j+\Big[\sum_{k=1}^{3}c_1^k g^{kk}\mu S^j_{kjk}\Big]u^j\Big\} \tag{17}$$
$$+\sum_{k=1}^{3}\Big\{c_1^k g^{kk}T^l_{kk}+\sum_{\substack{n=1\\k\neq n}}^{3}g^{nk}\Big[\mu u^i|_n\Big]\Big|_k+\sum_{\substack{n=1\\n\neq l}}^{3}g^{nl}\Big[\mu u^k|_n\Big]\Big|_k+(1-\delta^j_k)g^{ll}\Big[\mu u^k|_l\Big]_k\Big\}$$

where

$$\delta^j_1=\begin{bmatrix}1&0&0\\0&1&0\\0&0&1\end{bmatrix} \tag{18}$$

and

$$c^j_i=\begin{bmatrix}2&1&1\\1&2&1\\1&1&2\end{bmatrix} \tag{19}$$

and repeated indicies do not indicate summation.

Convective Terms

The convective term for the i-th equation can be written as

$$\rho u^j u^i\big|_j=\rho u^j\big[u^i{}_{,j}+u^m\Gamma^i_{mj}\big] \tag{20}$$

which becomes upon expansion

$$\rho u^j u^i\big|_j=\sum_{j=1}^{3}\Big\{\rho u^j u^i{}_{,j}+\sum_{m=1}^{2}\rho u^j u^m\Gamma^i_{mj}+\delta^j_3\sum_{n=1}^{3}\rho u^n u^j\Gamma^i_{nj}\Big\} \tag{21}$$

where the last term is nonzero only when j = 3. The full momentum equation is obtained by substituting Equations (17) and (21) into Equation (11) and treating the pressure gradient and velocity divergence as explicit terms. Since the pressure is specified and impressed upon the viscous layer, its specification replaces the normal momentum equation. Thus, the streamwise and spanwise momentum equations are the only two retained.

The momentum equation now becomes

$$\frac{\rho \partial u^i}{\partial t} = \sum_{j=1}^{3} \Big\{ \Big[c_1^j g^{jj} \mu \Big] u^i_{,jj} + \Big[c_1^j g^{jj} (\mu_{,j} + 2\mu \Gamma^i_{jl}) - \sum_{k=1}^{3} c_1^k g^{kk} \mu \Gamma^j_{kk} \Big] u^i{}_{,j}$$

$$+ \delta^j_l \Big[\sum_{k=1}^{3} c_1^k g^{kk} \mu_{,k} \Gamma^i_{kl} \Big] u^j + \Big[\sum_{k=1}^{3} c_1^k g^{kk} \mu S^i_{kjk} \Big] u^j - \tag{22}$$

$$\rho u^j u^i{}_{,j} + \sum_{m=1}^{2} \rho u^j u^m \Gamma^i_{mj} + \delta^j_3 \sum_{n=1}^{3} \rho u^n u^j \Gamma^i_{nj} \Big\}$$

$$+ \sum_{k=1}^{3} \Big\{ c_1^k g^{kk} T^i_{kk} + \sum_{\substack{n=1 \\ k \neq n}}^{3} g^{nk} \Big[\mu u^i \big|_n \Big] \big|_k + \sum_{\substack{n=1 \\ n \neq l}}^{3} g^{nl} \Big[\mu u^k \big|_n \Big] \big|_k$$

$$+ (1 - \delta^i_k) g^{ll} \Big[\mu u^k \big|_l \Big]_k \Big\}$$

Energy Equation

The energy equation employed here states that the stagnation temperature is constant throughout

$$T_o = T + \frac{1}{2} q^2 \tag{23}$$

The generalized tensor notation q^2 is given by

$$q^2 = u^i u^j g_{ij}$$

where u^i and u^j are the contravariant velocity components. Incorporating the assumptions made concerning the coordinate system employed, i.e.

$$g_{13} = g_{23} = 0$$

we obtain

$$q^2 = (u^1)^2 g_{11} + 2u^1 u^2 g_{12} + (u^2)^2 g_{22} + (u^3)^2 g_{33}$$

Neglecting the term involving $(u^3)^2$ with respect to the other terms, and defining physical velocity components, i.e.

$$u_p = u^1 h_1 \qquad\qquad w_p = u^2 h_2$$

we obtain

$$T_0 = T + \frac{1}{2}(u_p^2 + w_p^2) + \frac{g_{12}}{h_1 h_2} u_p w_p \tag{24}$$

This is the form of the energy equation used.

Equation of State

The equation of state assumes a perfect gas and is given by

$$P = \frac{\gamma - 1}{\gamma} \rho T \tag{25}$$

Linearizations

The following analyses assume a set of linear partial differential equations. However, the continuity equation and the convective part of the momentum equation are nonlinear, containing terms that involve the product of density and velocity components. In order to overcome this difficulty we employ the linearization procedure (described in Ref. 8 and reviewed in Appendix A) to linearize the aforementioned terms by Taylor series expansion about the known time level solution.

The density is first eliminated by employing the equations of state and energy, and thereafter the resulting terms are linearized. These terms are of the following form

$$\begin{aligned}(\rho\psi\theta)^{n+\beta} &= (\rho^n \psi^n)\theta^{n+\beta} + (\rho^n \theta^n)\psi^{n+\beta} \\ &+ \frac{\rho^n \psi^n \theta^n}{T^n}\left[(u^1)^n + \frac{g_{12}}{h_1 h_2}(u^2)^n\right](u^1)^{n+\beta} \\ &+ \frac{\rho^n \psi^n \theta^n}{T^n}\left[(u^2)^n + \frac{g_{12}}{h_1 h_2}(u^1)^n\right](u^2)^{n+\beta} \\ &+ \frac{\rho^n \psi^n \theta^n}{T^n}\left[2(T^n - T^0) + \left(\frac{\gamma}{\gamma-1}\right)\frac{p^{n+\beta}}{\rho^n} - 2\rho^n\psi^n\theta^n\right]\end{aligned} \tag{26}$$

where all velocity components are the contravariant ones, and θ is always a velocity component, (u^1, u^2, u^3) while ψ can be either a velocity component or a derivative of a velocity component. In the case when only one velocity term appears, i.e., ρu^i, we set $\psi^n = \psi^{n+\beta} = 1$.

It is important to note that in the preceeding equations the contravariant velocity components are used. However, as noted in Ref. 14, it appears advantageous to solve for the physical velocity components. Therefore, when the governing equations are subsequently cast into a form amenable to the application of the LBI scheme, they are transformed so that the physical velocity components appear.

The Turbulence Model

We treat the set of three-dimensional ensemble-averaged turbulent reduced Navier-Stokes equations. Ensemble averaging permits the appearance of low frequency (relative to the turbulence) time-dependent "mean" flow. It is, therefore, necessary to specify a turbulence model suitable for this problem.

The approach taken in the present effort assumes an isotropic turbulent viscosity, μ_T, relating the Reynolds' stress tensor to mean flow gradients.

$$\text{Reynolds stress} = \bar{\bar{\sigma}}_{Rey} = \frac{\mu_T}{Re}\left[\epsilon^{jk} - \frac{2}{3}\delta^j_j \Delta\right] \tag{27}$$

Using Favre averaging (Ref. 16), the governing equations then are identical to the laminar equations with velocity and density being taken as mean variables and viscosity being taken as the sum of the molecular viscosity, μ, and the turbulent viscosity, μ_T.

At this point we require additional closure assumptions for the Reynolds stresses, i.e., the evaluation of μ_T. There are a variety of approaches available, from the simpler mixing length models to the more complicated one and two-equation models. Since the intention here is to verify the code's performance in wall bounded cases, we chose the mixing length models which have worked well in the past for similar flow environments (Ref. 17). The extension to more complex models could be undertaken at a later time if warranted. At that time, the LBI procedure that is used for the solution of the momentum equation could be applied to the k and ε equations.

Employing the Prandtl mixing length concept, the turbulent viscosity is given as

$$\mu_T = \rho \ell^2 \epsilon^* \tag{28}$$

where ℓ is the mixing length, and ε^* is the mean strain, which for the general case is related to the dissipation function.

$$\epsilon^* = \sqrt{\Phi} \tag{29}$$

where Φ is the dissipation function. In Cartesian tensor notation Φ is given as

$$\Phi = 2e_{ij} \frac{\partial u_i}{\partial x_j} = 2 e_{ij} e_{ij} \tag{30}$$

where

$$e_{ij} = \frac{1}{2} \left[\frac{\partial u_i}{\partial x_j} + \frac{\partial u_j}{\partial x_i} \right]$$

In the case of two dimensions, Φ does not reduce directly to $\left|\frac{\partial u_1}{\partial x_3}\right|$ (where x_3 is normal to the wall) without the additional assumption that the other components are small.

In nonorthogonal coordinates, with generalized tensor notation employed, an analagous expression can be obtained for the dissipation function, i.e.

$$\Phi = e^{ij} u_i \big|_j \tag{31}$$

where

$$e^{ij} = g^{im} u^j \big|_m + g^{jm} u^i \big|_m \tag{32}$$

After some algebra, Φ reduces to

$$\Phi = \frac{1}{2} e^{ij} e_{ij} \tag{33}$$

where

$$e_{ij} = g_{ki} u^j \big|_m + g^{jm} u^i \big|_m$$

For computation purposes, Φ can be expressed somewhat simpler, i.e.

$$\Phi = \left[g^{im} u^j \big|_m + g^{jm} u^i \big|_m \right] g_{ik} u^k \big|_j \tag{34}$$

On expanding, and recalling that $g^{m3} = 0$ $m \neq 3$, Φ can be expressed as a summation

$$\Phi = \sum_k^3 \sum_j^3 u^j \big|_k u^k \big|_j + \sum_k^2 \sum_j^2 u^k \big|_j \left(\sum_i^2 \sum_m^2 g_{ik} g^{jm} u^i \big|_m \right) + g^{33} \sum_k^2 \sum_i^2 g_{ik} u^i \big|_3 u^k \big|_3 + g_{33} \sum_m^2 \sum_j^2 g^{jm} u^3 \big|_m u^3 \big|_j \tag{35}$$

$$+ g_{33} g^{33} u^3 \big|_3 u^3 \big|_3$$

As in the Cartesian tensor formulation, Φ does not automatically reduce to the dominant shear for two-dimensional boundary layers. Hence, provisions were made in the computer code that on option retains only the dominant component of the strain.

The mixing length formulation is based on the two-layer model

$$\begin{aligned} &\text{inner layer} && \ell_i = k y \mathcal{D} \\ &\text{outer layer} && \ell_o = \ell_\infty \end{aligned} \tag{36}$$

where y is the normal distance from the wall, $\mathcal{D}$ is the van Driest damping term

$$\mathcal{D} = 1 - \exp(-y^+/A^+)$$

and the von Karman constant k = .4 and the van Driest damping coefficient $A^+ = 26.0$. the dimensionless distance y+ is defined as

$$y^+ = \rho \frac{u_\tau y}{\mu}$$

and the friction velocity u_τ is taken as

$$u_\tau = (\tau_i/\rho)^{1/2}$$

In the outer layer ℓ_∞ is given by

$$\ell_\infty = \lambda \delta$$

where δ is the local boundary layer thickness defined as .995 u_e and $\lambda = .09$.

This form of the mixing length has a discontinuity in its first derivative at the matching point between ℓ_i and ℓ_o. An alternate form which avoids the discontinuity and varies smoothly between the two layers has been proposed by McDonald (Ref. 18), and is given by

$$\ell = \ell_\infty \tanh\left(\frac{\kappa y}{\ell_\infty}\right) \mathcal{D} \tag{37}$$

In the turbulent calculations to be presented we employ Eq. (37).

Spatial Difference Approximations

QR Operator Notation

In this section, implicit tridiagonal finite difference approximations to the first and second derivatives and to the spatial differential operator are considered. The QR operator procedure for generating a variety of spatial discretizations is also introduced. As special cases, standard second-order finite differences, first-order upwind differences, fourth-order operator compact implicit (OCI), fourth-order generalized OCI and exponential type methods are obtained. Since all these schemes are of the same form (cf. below), a single subroutine which defines the difference weights is all that is required to identify the method, while leaving

the basic structure of the program unaltered. Subsequently, the results of numerical experiments employing some of these schemes will be presented. The rationale for the use of the QR approach in the present problem is discussed in detail in Ref. 3.

The QR formulation allows for ADI methods and permits the treatment of systems of coupled equations, i.e., LBI methods. Although variable mesh schemes can be employed within the QR framework, it is believed preferable to use analytic transformations to obtain a uniform computational mesh, hence attention is restricted to uniform mesh formulations.

The general concepts and notation will be introduced for two-point boundary value problems and then the methodology will be extended to more general linear and nonlinear parabolic partial differential equations in one dimension. The application of the QR operator method to multidimensional problems is discussed in the section pertaining to the LBI scheme.

Consider the two-point boundary value problem

$$\tilde{L}(u) = \tilde{a}(x)u_{xx} + \tilde{b}(x)u_x + \tilde{c}(x)u = \tilde{f}(x) \tag{38}$$

with boundary values u(0) and u(1) prescribed. Derivative boundary conditions, although not discussed here, can easily be incorporated into the framework of the QR operator notation. Let the domain be discretized so that $x_j = (j-1)h$, $j = 1, 2, \ldots, J+1$, and $U_j \sim u(x_j)$, $F_j \sim u_x(x_j)$, $S_j \sim u_{xx}(x_j)$ and $h = 1/J$ is the mesh width. The numbering convention was chosen here to be compatible with FORTRAN coding.

Without loss in generality for $a(x) \neq 0$, Eq. (38) can be divided by a(x) so that we may treat instead the following equation

$$L(u) = u_{xx} + b(x)u_x + c(x)u = f(x) \tag{39}$$

where

$$b(x) = \tilde{b}(x)/\tilde{a}(x),\ c(x) = \tilde{c}(x)/\tilde{a}(x) \text{ and } f(x) = \tilde{f}(x)/\tilde{a}(x)$$

Substituting the finite difference approximations to the first and second derivatives

$$\frac{D_o}{2h}U_j = \frac{U_{j+1} - U_{j-1}}{2h} = F_j = u_x(x_j) + O(h^2) \tag{40}$$

$$\frac{D_+D_-}{h^2}U_j = \frac{U_{j-1} - 2U_j + U_{j+1}}{h^2} = S_j = u_{xx}(x_j) + O(h^2) \tag{41}$$

into Eq. (39) and rearranging, we obtain

$$L(u) \sim S_j + b_jF_j = \left[\frac{1}{h^2} - \frac{b_j}{2h}\right]U_{j-1} + \left[c_j - \frac{2}{h^2}\right]U_j + \left[\frac{1}{h^2} + \frac{b_j}{2h}\right]U_{j+1} = f_j \tag{42}$$

or

$$\left[1 - \frac{Rc_j}{2}\right] U_{j-1} + \left[h^2 c_j - 2\right] U_j + \left[1 + \frac{Rc_j}{2}\right] U_{j+1} = h^2 f_j \tag{43}$$

where $Rc_j = hb_j$ is the cell Reynolds number.

Equation (43) can be generalized by introducing operator format, i.e.,

$$r_j^- U_{j-1} + r_j^c U_j + r_j^+ U_{j+1} = h^2 (q_j^- f_{j-1} + q_j^c f_j + q_j^+ f_{j+1}) \tag{44}$$

where the superscripts (-) minus, (c) center, and (+) plus indicate the difference weight that multiplies the variable evaluated at the (j-1), (j) and (j+1) grid points respectively, and where the r_j's and q_j's for grid point j are functions of h, b_{j-1}, b_j, b_{j+1}, c_{j-1}, c_j and c_{j+1}. Comparing Eqs. (43) and (44) we can identify the r_j's and q_j's, viz.,

$$\begin{aligned} r_j^- &= 1 - Rc_j/2 & q_j^- &= 0 \\ r_j^c &= h^2 c_j - 2 & q_j^c &= 1 \\ r_j^+ &= 1 + Rc_j/2 & q_j^+ &= 0 \end{aligned} \tag{45}$$

We now define the tridiagonal difference operators Q and R

$$\begin{aligned} R\left[U_j\right] &= r_j^- U_{j-1} + r_j^c U_j + r_j^+ U_{j+1} \\ Q\left[f_j\right] &= q_j^- f_{j-1} + q_j^c f_j + q_j^+ f_{j+1} \end{aligned} \tag{46}$$

Noting that L(u) = f and substituting Eq. (46) into Eq. (44), we obtain

$$R\left[U_j\right] = h^2 Q\left[f_j\right] = h^2 Q\left[L(u)_j\right] \tag{47}$$

Alternatively by employing the inverse operator Q^{-1} and expression for $L(u)_j$ can be obtained

$$L(u)_j = \frac{1}{h^2} Q^{-1} R U_j \tag{48}$$

For standard central finite differences $Q = Q^{-1} = I$, the identity matrix, (the spatial operator is given explicitly in terms of U_{j-1}, U_j and U_{j+1}) so that nothing would appera to have been gained in obtaining Eq. (48). However, in general, for higher order methods whereas Q is tridiagonal Q^{-1} is a full matrix. Hence, Eq. (48) provides us with a convenient expression for the spatial operator for a wider class of difference approximations. The formalism in Eq. (48) is also applicable for first and second derivatives appearing alone (cf. Ref. 19). It should be pointed out, however, that Eq. (48) is not the most general formulation since the compact implicit formulas cannot be combined to yield a single scalar equation relating the spatial operator to the function values (Ref. 19).

In Refs. 3 and 20 a technique due to Berger, et al is described for constructing fourth order tridiagonal methods which possess a monotonicity property as the cell Reynolds number is increased, $R_c \to \infty$. A brief description of the method for deriving generalized OCI schemes is given in Appendix C and the resulting Q and R coefficients are presented in Table II.

Another family of schemes that can be expressed in QR operator notation are the so-called exponential methods. The idea, originally due to Allen (Ref. 21) (independently derived by Il'in (Ref. 22) and McDonald (Ref. 23)), and employed by Dennis (Ref. 24) is to set the difference weights so that the numerical solution is equated to the analytic solution for the locally frozen constant coefficient equation. The QR coefficients of this exponential scheme is given in Table III. This method is second order accurate for $Rc = O(1)$ and becomes first order accurate as $Rc \to \infty$ where the scheme reverts to first order upwind differencing.

Another exponential scheme which is uniformly second order accurate was developed by El-Mistikawy and Werle (Refs. 25 and 26). The "exponential box scheme" which is incorporated in their solution of the boundary layer equations with strong blowing, is based on a spatial operator of the form given in Eq. (39). Berger, et al (Ref. 27) derived the counterpart for an operator of the form given in Eq. (30), but with $c = 0$. The Q and R coefficients are presented in Table IV. Although this scheme reverts to second order upwind differences as $Rc \to \infty$, it does not possess a discrete maximum principle while the exponential scheme of Allen (Ref. 20) does. In Table V a centered finite difference scheme is presented which permits the addition of artificial dissipation to the spatial operator when $|Rc| > Rc_{max}$ so that $|Rc|$ never exceeds Rc_{max}.

Application to Coupled Nonlinear Parabolic Equations

Before considering the LBI technique, we discuss some of the limitations placed on the QR operator scheme in solving a system of nonlinear parabolic equations.

Given a system of m nonlinear parabolic equations in m unknowns,

$$\sum_{i=1}^{m} \left\{ \frac{1}{a_{ij}^{n+\beta}} \frac{(u_{ij}^{n+1} - u_{ij}^{n})}{\Delta t} - N_i^{n+\beta}(u_1, u_2, \ldots u_m, x_1, x_2, x_3, t) \right\} = 0$$

$$j = 1, 2, \ldots, J+1$$

where $N_i^{n+\beta}$ is a quasilinear spatial operator, the QR formalism carries directly over provided that for any equation only one independent variable is operated upon by the differential operator. For example,

$$\frac{1}{a(u,w,v)} u_t = u_{xx} + b(u,v,w)u_x + c(u,v,w)$$

is allowed since x derivatives of u only appear, while

$$\frac{1}{a(u,w,v)} u_t = u_{xx} + b(u,v,w)u_x + c(u,v,w) + d(u,v,w)w_x$$

is not allowed since x derivatives of both u and w appear. The approximate form of unsteady Navier-Stokes equations used here, when written in quasi-linear form, falls within the class of allowable differential operators. Thus, for the problem being addressed in the present study, the OCI schemes are applicable. Note that within the splitting approach, non allowable terms in the OCI scheme such as dw_x above, may be split off and treated by a special implicit sweep. Provided care is taken and for instance the Douglas-Gunn formalism is adhered to, no particular problem arises other than the cost of an additional implicit sweep which is incurred.

Thus, multidimensional problems and/or more general equation forms can usually be accomodated by a splitting procedure, which reduces the differential operator to a sequence of one-dimensional problems which have the appropriate allowable form.

However, as with standard finite differences, to avoid the cost of additional implicit sweeps, special procedures must be applied to cross derivative terms, e.g., extrapolation or explicit treatment.

Linearized Block Implicit Scheme

Consider a system of nonlinear partial differential equations

$$A\vec{\Phi}_t = \mathcal{D}\vec{\Phi} + \vec{\Psi} \tag{49}$$

where $\vec{\Phi}$ is a vector of unknowns and $\vec{\Psi}$ is a source term vector which is a function of x^1, x^2, x^3 and t. Extension to source terms which are functions of $\vec{\Phi}$ are discussed in Ref. (8). $\mathcal{D}$ is a three-dimensional nonlinear differential operator and the matrix A appearing in the momentum equations is equal to ρI where ρ is the density and I the unity matrix.

Equation (49) may be centered abut the $n+\beta$ time level, i.e. $t^{n+\beta} = (n+\beta)\Delta t = n\Delta t+\beta\Delta t = t^n+\beta\Delta t$, and written

$$A^{n+\beta}\left[\vec{\Phi}^{n+1} - \vec{\Phi}^n\right]/\Delta t = \mathcal{D}^{n+\beta}\vec{\Phi}^{n+\beta} + \vec{\Psi}^{n+\beta} \tag{50}$$

where $0 \leq \beta \leq 1$ is a parameter allowing one to center the time step, i.e., $\beta = 0$ corresponds to a forward difference, $\beta = 1/2$ to Crank-Nicolson and $\beta = 1$ to a backward difference.

After linearizing Equation (50) by Taylor series expansion in time about the n^{th} time level by the procedure described in Ref. 8 to give a second-order linearization, we obtain

$$A^n\left[\vec{\Phi}^{n+1} - \vec{\Phi}^n\right]/\Delta t = \mathcal{L}^n\left[\vec{\Phi}^{n+\beta} - \vec{\Phi}^n\right] - \mathcal{D}^n\vec{\Phi}^n + \vec{\Psi}^{n+\beta} \tag{51}$$

where $\mathcal{L}$ is the linearized differential operator obtained from $\mathcal{D}$ by Taylor Series expansion in time.

The difference between the nonlinear operator $\mathcal{D}$ and the linear operator $\mathcal{L}$ is defined as $M^n = \mathcal{D}^n - \mathcal{L}^n$. At the intermediate level $n + \beta$, $\Phi^{n+\beta}$ is represented as

$$\vec{\Phi}^{n+\beta} = \beta\vec{\Phi}^{n+1} + (1-\beta)\vec{\Phi}^n \tag{52}$$

Using these relationships and dropping the vector superbar for convenience a two-level hybrid implicit-explicit scheme is obtained

$$A^n(\Phi^{n+1}-\Phi^n)/\Delta t = \beta\mathcal{L}^n(\Phi^{n+1}-\Phi^n) + \mathcal{L}^n\Phi^n + M^n\Phi^n + \Psi^{n+\beta} \tag{53}$$

The vector $\psi^{n+\beta}$ represents all of the terms in the system of equations which are treated explicitly. More about this will be said later, but for the moment note that $\psi^{n+\beta}$ may be approximated to the requisite order of accuracy by some multilevel linear explicit relationship, or approximated by ψ^n with a consequent order reduction in temporal accuracy.

The operator $\mathcal{L}$ is now expressed as a sum of convenient, easily invertible suboperators $\mathcal{L} = \mathcal{L}_1 + \mathcal{L}_2 + \ldots \mathcal{L}_m$. In the usual ADI framework these suboperators are associated with a specific coordinate direction. Further, it is supposed that these suboperators can be expressed in the QR notation introduced earlier. Writing $\psi^{n+\beta}$ and $M^n\phi^n$ as a single source term $S^{n+\beta}$, Equation (45) is written as

$$A^n\left[\Phi^{n+1}-\Phi^n\right]/\Delta t = \beta\left[\mathcal{L}_1^n + \mathcal{L}_2^n + \mathcal{L}_3^n\right]\left[\Phi^{n+1}-\Phi^n\right] + \left[\mathcal{L}_1^n+\mathcal{L}_2^n+\mathcal{L}_3^n\right]\Phi^n + S^{n+\beta} \tag{54}$$

To solve this system efficiently it is split into a sequence of easily invertible operations following a generalization of the procedure of Douglas and Gunn (Ref. 19) in its natural extension to systems of partial differential equations. The Douglas-Gunn splitting of Eq. (54) is written as the following three-step procedure

$$A^n\left[\Phi^*-\Phi^n\right]/\Delta t = \beta\mathcal{L}_1^n(\Phi^*-\Phi^n) + \left[\mathcal{L}_1^n+\mathcal{L}_2^n+\mathcal{L}_3^n\right]\Phi^n + S^{n+\beta}$$

$$A^n\left[\Phi^{**}-\Phi^n\right]/\Delta t = \beta\mathcal{L}_1^n\left[\Phi^*-\Phi^n\right] + \beta\mathcal{L}_2^n\left[\Phi^{**}-\Phi^n\right] + \left[\mathcal{L}_1^n+\mathcal{L}_2^n+\mathcal{L}_3^n\right]\Phi^n + S^{n+\beta} \tag{55}$$

$$A^n\left[\Phi^{***}-\Phi^n\right]/\Delta t = \beta\mathcal{L}_1^n\left[\Phi^*-\Phi^n\right] + \beta\mathcal{L}_2^n\left[\Phi^{**}-\Phi^n\right] + \beta\mathcal{L}_3^n\left[\Phi^{***}-\Phi^n\right] + \left[\mathcal{L}_1^n+\mathcal{L}_2^n+\mathcal{L}_3^n\right]\Phi^n + S^{n+\beta}$$

which can be transformed to the alternative form

$$\begin{aligned}
\left[A^n - \Delta t\,\beta \mathcal{L}_1^n\right]\left[\Phi^* - \Phi^n\right] &= \Delta t\left[\mathcal{L}_1^n + \mathcal{L}_2^n + \mathcal{L}_3^n\right]\Phi^n + \Delta t\, S^{n+\beta} \\
\left[A^n - \Delta t\,\beta \mathcal{L}_2^n\right]\left[\Phi^{**} - \Phi^n\right] &= A^n\left[\Phi^* - \Phi^n\right] \\
\left[A^n - \Delta t\,\beta \mathcal{L}_3^n\right]\left[\Phi^{***} - \Phi^n\right] &= A^n\left[\Phi^{**} - \Phi^n\right]
\end{aligned} \tag{56}$$

If the intermediate levels are eliminated, the scheme can be written in the so-called factored form

$$\begin{aligned}
&(A^n - \beta\,\Delta t\,\mathcal{L}_1^n)(A^n)^{-1}(A^n - \beta\,\Delta t\,\mathcal{L}_2^n)(A^n)^{-1}(A^n - \beta\,\Delta t\,\mathcal{L}_3^n)(\Phi^{n+1} - \Phi^n) = \\
&\Delta t(\mathcal{L}_1^n + \mathcal{L}_2^n + \mathcal{L}_3^n)\Phi^n + \Delta t\, S^{n+\beta}
\end{aligned} \tag{57}$$

At this point it becomes necessary to consider the structure of the operators $\mathcal{L}_1$, $\mathcal{L}_2$ and $\mathcal{L}_3$. It will be recalled from the one-dimensional scalar problem that use of the QR format greatly facilitated the introduction of a wide variety of spatial difference formulae. It follows that in the extention to multidimensions undertaken here, the use of the QR formulation results in the appearance of the inverse operator Q^{-1} with the sub-blocks of the $\mathcal{L}_1$, $\mathcal{L}_2$, $\mathcal{L}_3$ operators. In order to implement the scheme the inverse operator Q^{-1} must be cleared. Accordingly, the scalar operator Q is generalized to the vector operator $\vec{Q}_i$ with (diagonal) sub-blocks Q_{ji}. In this generalization j = 1, 2 apply to the momentum equations and j = 3 applies to the continuity equation. The i subscript is associated with the coordinate directions of the $\mathcal{L}_i$ operators. The discretization results in one diagonal sub-block for each grid point for each of the three $\vec{Q}_i$. Each intermediate step of the algorithm is now premultiplied by the $\vec{Q}_i$ associated with the $\mathcal{L}_i$ implicit operator. Writing the product operator $\vec{Q}_i\,\mathcal{L}_i$ as L_i, the inverse operators are thus removed and the scheme is written, once again dropping the vector superscript for convenience

$$\begin{aligned}
\left[Q_1 A^n - \Delta t\,\beta L_1^n\right]\left[\Phi^* - \Phi^n\right] &= \Delta t\, L_1\,\Phi^n + \Delta t\, Q_1\left[\mathcal{L}_2^n + \mathcal{L}_3^n\right]\Phi^n + \Delta t\, Q_1 S^{n+\beta} \\
\left[Q_2 A^n - \Delta t\,\beta L_2^n\right]\left[\Phi^{**} - \Phi^n\right] &= Q_2 A^n\left[\Phi^* - \Phi^n\right] \\
\left[Q_3 A^n - \Delta t\,\beta L_3^n\right]\left[\Phi^{***} - \Phi^n\right] &= Q_3 A^n\left[\Phi^{**} - \Phi^n\right]
\end{aligned} \tag{58}$$

$$\mathcal{L}_2^n\Phi^n = Q_2^{-1} R_2 \Phi^n \qquad \mathcal{L}_3^n\Phi^n = Q_3^{-1} R_3 \Phi^n$$

$$\Phi^{n+1} = \Phi^{***} + O(\Delta t^3)$$

With the removal of the inverse operator Q^{-1}, the question of the proper intermediate level solution boundary conditions can be addressed. As is pointed out by Briley and McDonald (Ref. 2), the proper intermediate level boundary conditions may be derived by running through the intermediate steps in reverse order. Defining a boundary condition operator B_i^n after linearizing the appropriate physical boundary condition by Taylor series expansion in time as

$$B_i^n(\Phi^{n+1}) = g(t, \Phi^n)$$

and applying this operator to the algorithm defines the boundary conditions as

$$\begin{aligned} B_3^n Q_3 A^n\left[\Phi^{**} - \Phi^n\right] &= \left[B_3^n Q_3 A^n - \Delta t \beta B_3^n L_3^n\right]\left[\Phi^{***} - \Phi^n\right] \\ B_2^n Q_2 A^n\left[\Phi^{*} - \Phi^n\right] &= \left[B_2^n Q_2 A^n - \Delta t \beta B_2^n L_2^n\right]\left[\Phi^{**} - \Phi^n\right] \end{aligned} \tag{59}$$

Note that unless $B_i^n L_i^n$ commute (an unlikely event except with Dirchilet boundary conditions, where $B_i^n = I$) the exact boundary conditions cannot be derived. A number of possible strategies are possible at this point aimed at various levels of approximation to $B_i^n L_i^n$. For the present, the term $\Delta t \beta B_i^n L_i^n[\Phi - \Phi^n]$ is neglected. This introduces an error of order $O[\Delta t(\Phi - \Phi^n)]$ into the solution but note that this error disappears at steady state where $\Phi^{***} = \Phi^{**} = \Phi^*$. Neglect of the $\Delta t \beta B_i^n L_i^n [\Phi - \Phi^n]$ term is, of course, equivalent to applying the physical boundary conditions on the intermediate level variables.

This completes the general derivation of the algorithm and attention is now given to the specific forms of the L_i^n operators including the rather special form of the component operator for the continuity equation.

It is worth noting that the operator $\mathcal{D}$ or $\mathcal{L}$ can be split into any number of components which need not be associated with a particular coordinate direction. As pointed out by Douglas and Gunn (Ref. 19), the criterion for identifying sub-operators is that the associated matrices be "easily solved" (i.e., narrow-banded). Thus, mixed derivatives and the complicating terms which might inhibit the use of OCI can be treated implicitly within such a framework, although this would increase the number of intermediate steps and thereby complicate the solution procedure.

An inspection of Eq. (58) reveals that only the linearized operators L_1^n, L_2^n and L_3^n appear. Indeed, the computer code employs this feature by evaluating these three

operators before the first sweep, storing them and accessing them as needed in the subsequent three sweeps. In addition, the terms arising from the nonlinear terms are immediately absorbed into $S^{n+\beta}$ as they appear, allowing for an efficient evaluation of the terms in the differential equations.

The spatial operators appearing in the differential equations are $\mathcal{L}_1^n$, $\mathcal{L}_2^n$ and $\mathcal{L}_3^n$ must be identified at least formally in order to isolate the coefficients that are to be used in the construction of the Q and R operators. The operators $\mathcal{L}_1^n$, $\mathcal{L}_2^n$, $\mathcal{L}_3^n$ can be represented in standard form at each grid point, i.e.,

$$\mathcal{L}^n{}_i \Phi_i^n = a_{11}^n \Phi_{i,11} + a_{12}^n \Phi_{i,1} + a_{13}^n \Phi_i + a_{14}^n \Phi_2 + a_{15}^n \Phi_3 \qquad (60)$$

In Eq. (60) the first subscript of Φ indicates the velocity component (associated with the corresponding direction and " , " indicates a derivative. The subscripts of the a_{ij}^n refer to the direction (i) and the term in the equation (j) respectively. Note that the equation is in quasi-linear form, since the coefficients of the derivative operators need to be identified, for use with the QR operator technique employed here. Alternate schemes have been proposed by Leventhal (Ref. 28) for equations in conservation form but are not considered here. In the following section, a description will be given of how this entire operator is discretized by employing the QR operator format, and how the discretization is incorporated into the LBI framework in order to solve the system of equations (58).

The continuity equation is considered first. Since it is a first-order partial differential equation it does not have the standard form of Eq. (59). Furthermore, in the linearization process ρ has been eliminated in favor of the u^i velocity components so that the continuity equation has become an equation for the three velocity components, and not density.

An inspection of the system of equations under consideration reveals that substantial savings can be realized if the equations are partioned appropriately. This is in keeping with the observations of McDonald and Briley (Ref. 8) who noted that skillful partioning of the resulting matrix can lead to significant decreases in computation time. Due to the use of a boundary layer coordinate system, the normal velocity appears only in conjunction with terms associated with the normal "3" direction in the two momentum equations. Hence, in the first two sweeps one is required to solve only for the two corresponding velocity components the streamwise and spanwise momentum equation without the need of considering the continuity equation. However, on the third sweep where all 3 velocity components appear, one must solve all 3 equations. This strategy reduces the solution procedure to the inversion of

two 2 x 2 block matrices and one 3 x 3 block matrix rather than three 3 x 3 block matrices which leads to a substantial reduction in computation time. If the full Navier-Stokes equations were considered (including a normal momentum equation) the aforementioned partioning could not be applied since the normal velocity would appear in all three sweeps.

The question that arises is how to appropriately split the continuity equation, since it is solved only on the third sweep. Here again the Douglas-Gunn formulation leads to the appropriate choice. The continuity equation written in conservation form is,

$$\frac{\partial \rho}{\partial t} + \frac{1}{J} \frac{\partial}{\partial x^1} \left[J \rho u^1 \right] = 0 \tag{61}$$

After linearizing and eliminating ρ, the increment form is obtained

$$\begin{aligned} A^n \Delta u^{n+1} + B^n \Delta w^{n+1} + \frac{\Delta t \beta}{J} \frac{\partial}{\partial x^3} \left[v^n A^n \Delta u^{n+1} + v^n B^n \Delta w^{n+1} + \rho^n \Delta v^{n+1} \right] \\ = - \frac{\Delta t}{J} \frac{\partial}{\partial x^1} \left[J \rho u^1 \right]^n + \frac{\Delta t \beta}{J} \frac{\partial}{\partial x^1} \left[(\rho^n + u^n A^n) \Delta u^{n+1} + (u^n B^n) \Delta w^{n+1} \right] \\ + \frac{\Delta t \beta}{J} \frac{\partial}{\partial x^2} \left[(\rho^n + w^n B^n) \Delta w^{n+1} + (w^n A^n) \Delta u^{n+1} \right] \end{aligned} \tag{62}$$

where all the veloicty components are the contravariant components $u = u^1$, $w = u^2$ and $v = u^3$. J. is the Jacobian and

$$A^n = \frac{\rho^n}{T^n} \left[g_{11} u^n + g_{12} w^n \right]$$

$$B^n = \frac{\rho^n}{T^n} \left[g_{22} w^n + g_{12} u^n \right]$$

By employing the Douglas-Gunn procedure, Equation (62) is represented as a third sweep equation, and a consistent approximation is obtained to the continuity equation, i.e., the x^1 derivative term is evaluated at the * level and the x^2 derivative

term is evaluated at the ** level. The values of the intermediate derivative terms are obtained after the solution of the first two sweeps of the two momentum equations. Note that these terms do not contain the normal velocity. The equation can thus be written in symbolic form

$$A^n \Delta u^{n+1} + B^n \Delta w^{n+1} + \frac{\Delta t \beta}{J} \frac{\partial}{\partial x^3} \left[J \left\{ A^n v^n \Delta u^{n+1} + v^n B^n \Delta w^{n+1} + \rho^n \Delta v^{n+1} \right\} \right] \tag{63}$$

$$= S^n - \beta \frac{\Delta t}{J} \frac{\partial}{\partial x^1} \left[J \{ \} \right]^* - \beta \frac{\Delta t}{J} \frac{\partial}{\partial x^2} \left[J \{ \} \right]^{**}$$

Since the only term involving v is in the x^3 derivative term, one can directly integrate the equation with respect to x^3, i.e.

$$\int_{x^3} \left[A^n \Delta u^{n+1} + B^n \Delta w^{n+1} \right] dx^3 + \Delta t \frac{\beta \Delta t}{J} \left[v^n A^n \Delta u^{n+1} + v^n B^n \Delta w^{n+1} + \rho^n \Delta v^{n+1} \right]$$

$$= \int_{x^3} \left\{ S^n - \frac{\beta \Delta t}{J} [\ ]^* - \frac{\beta \Delta t}{J} [\ ]^{**} \right\} dx^3 .$$

The next section describes how this is done very easily via the QR operator scheme. The concept of integrating directly the continuity equation is not now. Davis (Ref. 29) in his coupled procedure for the solution of two-dimensional steady boundary layer equation used a trapezoidal rule to integrate the continuity equation. Weinberg (Refs. 30 and 31) also used a fourth order Simpson integration scheme to solve the compressible boundary layer equations. Such procedures are stable and offer a viable alternative to approximating the derivatives by finite differences. Note that conceptually the continuity equation in integrated form is treated on each sweep of the Douglas-Gunn splitting, although in actuality this can be viewed as having the same form as each sweep and the integration operator can be incorporated into the $\mathcal{L}$ and $\mathcal{D}$ difference operators, and as a result the stability and consistency of the original splitting is retained.

Implementation of the LBI Scheme Employing the QR Operator Technique

Consider the third sweep of Equation (57) in which both momentum equations and the continuity equation are solved. The momentum equations are in the form

$$\left[A^n - \beta\Delta t \mathcal{L}_3^n\right]\Delta\Phi^{***} = A^n\Delta\Phi^{**} \tag{64}$$

where $\Delta\Phi^{***}$ is the column vector of unknowns, u, v, w. Here it has been implicitly assumed that the equations have been appropriately normalized and that the contravariant velocity components have been suitably transformed into their physical components. Employing physical components, (cf. Ref. 32) leads to a better behaved solution since these components are not unduly influenced by geometrical variations.

For the streamwise momentum equation one obtains

$$\mathcal{L}_3^n\,\Delta\Phi^{***} = \Delta u_{,33} + a_{23}\Delta u_{,3} + a_{33}\Delta u + a_{43}\Delta w + a_{53}\Delta v \tag{65a}$$

while for the spanwise momentum equation one obtains

$$\mathcal{L}_3^n\,\Delta\Phi^{***} = \Delta w_{,33} + b_{23}\Delta w_{,3} + b_{33}\Delta w + b_{43}\Delta v + b_{53}\Delta u \tag{65b}$$

where superscript *** has been omitted from Δu, Δv and Δw. Now in Equation (65a), the first three terms on the right-hand side are approximated by the operator equivalent

$$\Delta u_{,33} + a_{23}\Delta u_{,3} + a_{33}\Delta u \quad = \quad \frac{Q_1^{-1}R_1}{\Delta x_3^2}\,\Delta u \tag{66}$$

so that

$$\mathcal{L}_3^n\,\Delta\Phi^{***} = \frac{Q_1^{-1}R_1\Delta u}{\Delta x_3^2} + a_{43}\Delta w + a_{53}\Delta v \tag{67}$$

Similar approximations are made for Equation (65b). After substituting Equation (66) into Equation (64), and multiplying thru by Q, one obtains for the streamwise momentum equation

$$\left[Q_1\rho^n - \beta\lambda R_1\right]\Delta u - \beta\Delta t\, Q_1 a_{43}\Delta w - \beta\Delta t\, Q_1 a_{53}\Delta v = Q_1\rho^n\Delta u^{**} \tag{68}$$

where $\lambda = \Delta t/\Delta x_3^2$

Similarly for the spanwise momentum equation, one obtains

$$\left[Q_2\rho^n - \beta\lambda R_2\right]\Delta w - \beta\Delta t\, Q_2 b_{43}\Delta v - \beta\Delta t\, Q_2 b_{53}\Delta u = Q_2\rho^n\Delta w^{**} \tag{69}$$

The same type of procedure is employed for the continuity equation. Since the continuity equation involves only first derivatives, they can be represented as

$$\frac{\partial}{\partial x^3} = \frac{Q_C^{-1}R_C}{\Delta x_3} \tag{70}$$

The operators Qc and Rc are constructed to approximate the weights associated with either a second order trapezoidal rule or a fourth order Simpson's rule, i.e.

Trapezoidal rule

$$q_c^- = 0 \ , \ q_c^c = \frac{1}{2} \ , \ q_c^+ = \frac{1}{2}$$

$$r_c^- = 0 \ , \ r_c^c = -1 \ , \ r_c^+ = 1$$

Simpson's rule

$$q_c^- = \frac{1}{3} \ , \ q_c^c = \frac{4}{3} \ , \ q_c^+ = \frac{1}{3}$$

$$r_c^- = -1 \ , \ r_c^c = 0 \ , \ r_c^+ = 1$$

The discretized continuity equation thus becomes

$$JA^n\Delta u + JB^n\Delta w + \frac{\Delta t\beta}{\Delta x_3} Q_c^{-1} R_c\left[JA^n v^n\Delta u + JB^n v^n\Delta w + J\rho^n\Delta V\right] = RHS \qquad (71)$$

where RHS contains all the terms due to the linearization procedure and the terms evaluated at the * and ** levels. Multiplying thru by Q_c and setting $\omega = \Delta t/\Delta x_3$, the equation reduces to

$$\left[Q_c JA^n + \beta\omega R_c JA^n v^n\right]\Delta u + \left[Q_c JB^n + \beta\omega R_c JB^n v^n\right]\Delta w + \left[\beta\omega R_c J\rho^n\right]\Delta V = Q_c(RHS) \qquad (72)$$

The resulting matrix derived from Equations (67), (68) and (71) becomes a block 3 tridiagonal matrix (Q and R are tridiagonal operators) with each sub block taking on the form

$$\begin{bmatrix} \left[\ Q_1\rho^n - \beta\lambda R_1\ \right] & \left[\ -\beta\Delta t\, Q_1 a_{43}\ \right] & \left[-\beta\Delta t Q_1 a_{53}\right] \\ \left[\ -\beta\Delta t\, Q_2 b_{53}\ \right] & \left[\ Q_2\rho^n - \beta\lambda R_2\ \right] & \left[-\beta\Delta t Q_2 b_{43}\right] \\ \left[Q_c JA^n + \beta\omega R_c JA^n v^n\right] & \left[Q_c JB^n + \beta\omega R_c JB^n v^n\right] & \left[\beta\omega R_c J\rho^n\right] \end{bmatrix} \begin{bmatrix} \Delta u \\ \Delta w \\ \Delta v \end{bmatrix} = \begin{bmatrix} Q_1(\Delta u^{**}) \\ Q_2(\Delta w^{**}) \\ Q_c(RHS) \end{bmatrix}$$

This matrix is inverted by standard LU decomposition.

Boundary Conditions and Initial Conditions

The type of boundary conditions employed in the solution of the approximate form of the Navier-Stokes equations are described in this section. On the body surface no-

slip is prescribed for all the velocity components. At the outer edge of the viscous layer the magnitudes of the streamwise and spanwise velocity components are also prescribed. However, the value of the normal velocity component is not set, but rather computed as part of the numerical solution as is the practice in standard boundary layer procedures.

At the inflow boundaries, (upstream) velocity profiles are fixed, while extrapolation conditions are employed at the outflow boundaries (downstream). Further discussion of this matter is given in the section of numerical results.

The intermediate boundary conditions employed on the first two sweeps are the physical ones. For steady multidimensional problems, the imposition of physical intermediate boundary conditions did not impair the quality of the solutions obtained. These results are in keeping with the analysis of McDonald and Briley (Ref. 2) for second order spatial schemes. For the unsteady cases considered physical intermediate boundary conditions have also been used without any apparent difficulty.

The question of proper intermediate boundary conditions for fourth order methods until recently has not been resolved. Fairweather and Mitchell (Ref. 33) developed nonphysical intermediate boundary conditions for a fourth order solution of Laplace's equation, and showed that, in general, the use of noncorrected, i.e., physical boundary conditions leads to a loss in steady state accuracy for their method. As pointed out by Fairweather and Mitchell (Ref. 33), their scheme is inconsistent. It is this inconsistency that requires one to use appropriately derived intermediate boundary conditions in order to recover a steady state solution independent of time. However, if a consistent scheme were to be used, e.g. Douglas-Gunn, then physical boundary conditions can be applied without any loss in steady state accuracy, including fourth order generalized OCI schemes. These conclusions generalize the results obtained by Briley and McDonald (Ref. 2) for second order finite difference methods to higher order schemes and to those schemes that can be cast into a QR operator framework. However, using physical intermediate boundary conditions is expected to decrease the overall temporal accuracy to first order.

The Computer Code

The type of numerical algorithm employed as well as its formulation has a marked impact on the structure of the computer code. One needs to consider both the number of CPU operations as well as the memory requirements. Usually, the number of operations can be reduced at the expense of increasing the amount of storage. However, for three-dimensional problems the accessible fast (small core)

memory becomes a severe limitation even in the case where the code has not been modified to optimize the operation count.

The storage requirements for the solution of the approximate form of the three-dimensional Navier-Stokes equations for even modest size grids (e.g. 30 x 30 x 30) exceed the available small core memory of a machine like the CDC 7600. One must then resort to either mass storage devices such as disks or slow access memory (large core).

In using such devices both access time and transfer rates must be considered. When small amounts of data are being transferred frequently then access time becomes a significant factor. Therefore, a combination of strategies must be employed in order to optimize both access time and transfer rate.

An investigation of the operation count of the LBI scheme in conjunction with the QR operator technique leads to the conclusion that the most significant fraction of time is spent in computing the matrix coefficients, i.e. the linearization coefficients and difference weights. This amount far exceeds the time required for the matrix inversion. Hence, it is worthwhile to optimize the calculation of these coefficients, and if possible store their values. This procedure was accomplished by storing the operator coefficients $\mathcal{L}_2^n$ and $\mathcal{L}_3^n$ as they were computed in the first sweep on the right-hand side of the differential equation. On the second and third sweeps $\mathcal{L}_2^n$ and $\mathcal{L}_3^n$ were accessed respectively and were not recomputed. It was for this reason that the formulation of the LBI scheme referred to the linearized operators $\mathcal{L}_i^n$'s instead of the $\mathcal{D}_i^n$'s on the right-hand side of the equation.

In order to minimize data transfer, the code was constructed to have in memory one plane of data at any given time. Recall that 1-2 planes are parallel to the surface while the 3 direction is normal to the surface. During the solution procedure, which is described below, the first and second sweeps are conducted on 1-2 planes, evaluated in sequence in the 3 direction from the surface to the outer edge. The third sweep is conducted on 1-3 planes evaluated in sequence in the 2 direction.

A problem arises in two dimensions during the first sweep, in that only the '1' or streamwise direction is required yet '1-2' planes must be solved sequentially. This means that only '1' lines are solved in the first sweep since the '2' direction is essentially passive, and thus leads to unnecessary data transfer. In order to alleviate this inefficiency the code was modified so that in two dimensions the equations would be solved 'in core' in the '1-3' plane on both sweeps. At the same time, additional modifications were introduced that resulted in a significant speed up of the code. These include specialized hard wired 2 x 2 and 3 x 3 block matrix multipliers and inverters, and an efficient addressing routine for spatially dependent variables. As a result of including these modifications, the CPU time for

two-dimensional problems was reduced by nearly an order of magnitude. The run time for a two-dimensional turbulent calculation is .00063 sec per grid point per time step and for a laminar two-dimensional calculation is .00055 sec per grid point per time step. Although there are still additional modifications remaining to be incorporated into the code, it is believed that the major gains in efficiency have already been obtained.

The general structure of the computer code will now be described. After the input section and the initialization of data e.g. geometry, grid transformations, flowfield, etc. the actual construction of the difference operators is begun. The first derivatives of the velocity components and viscosity are obtained for the entire flow field and stored for ready access when needed for the computation of the appropriate terms in the governing equations. Thereafter the terms that are to be treated explicitly are evaluated and absorbed into the function S^n.

The operators $\mathcal{L}_1$, $\mathcal{L}_2$ and $\mathcal{L}_3$ are then computed. These are used to evaluate the appropriate Q and R coefficients which are then stored for easy retrieval during each of the ADI sweeps.

In the first sweep the matrix resulting from the application of the $\mathcal{L}_1$ operators for the streamwise and spanwise momentum equation is solved as a 2 x 2 coupled system. The solution of this system, the * level quantities, are then used to construct the right-hand side of the second sweep equations and to evaluate the appropriate * level term in the continuity equation. At this point the $\mathcal{L}_2$ operator is accessed and again a 2 x 2 system of equations for the streamwise and spanwise momentum equation is solved. The ** level quantities are then used to construct the right-hand side of the third sweep equations as well as the appropriate terms in the continuity equation. For the third sweep equations which consist of the two momentum equations and the continuity equation, the $\mathcal{L}_3$ operator is accessed from memory. The resulting 3 x 3 system of equations is solved for the three velocity components.

After the primary variables are evaluated, the theromodynamic quantities, density, temperature and viscosity are computed. The procedure is then repeated at the following time steps.

It is noteworthy that the scheme just described operates on vectors, i.e. lines of data. Therefore, it could show promise for vectorized machines.

Numerical Results

In this section we describe results of numerical computations that were obtained by exercising the computer code discussed previously. The objectives of these calculations are; to demonstrate the viability of the code in performing two dimensional steady turbulent flow calculations as well as in computing two dimensional unsteady flows, to compare second order finite differences with fourth order methods, to discover any limitations of the solution procedure and to indicate what modifications would be recommended to improve the code's performance.

In meeting these goals initial calculations were performed with the fourth order generalized OCI scheme. Model one and two dimensional problems were considered, progressing to the solution of the laminar boundary layer equations. These calculations which included both the Blasius and Howarth flows were used to validate the fourth order generalized OCI option as well as the code modifications described in the previous section.

At this point the choice of the specific calculations to be considered was addressed. The first set of calculations consisted of two turbulent cases; zero pressure gradient (Weighardt Flat Plate (Ref. 34)) and adverse pressure gradient leading to separation (Newman Airfoil (Ref. 34)). These cases were chosen due to the reliable experimental data that are available with which comparisons can be made. The second set of calculations treat the laminar two dimensional oscillating flow over a flat plate. Here again there is abundant information (theoretical as well as computational) with which to make meaningful comparisons.

Two-Dimensional Steady Turbulent Flow

Weighardt Flat Plate

The first case we consider is the turbulent flow over a plat plate with zero pressure gradient. Flow conditions were specified to match with the experimental data of Weighardt (Case 1400 in Ref. 34), viz.

$$u_e = 108 \text{ ft/sec.}$$

$$R_e = 661{,}190/\text{ft.}$$

The computational domain was chosen with the inflow boundary located at $x = .6135$ ft and the outflow boundary located at $x = 13.1232$ ft, while the outer edge was set to a constant value of $y = .25$ ft for all x. In order to resolve the sublayer two types of grid transformation were employed, a Roberts type (Ref. 11)

which is essentially a hyperbolic tangent function and an Oh type (Ref. 35) which is constructed from a series of complimentary error functions. In the streamwise direction a uniform grid distribution was employed. The total grid distribution consisted of 36 points in each direction.

At the inflow boundary the velocity profiles are required to be specified. These were obtained directly from Weighardt's data by using a Coles' law profile (Ref. 34) i.e.

$$\left.\begin{aligned} \frac{u}{u_\tau} &= \frac{1}{\kappa}\ln\left(\frac{yu_\tau}{\upsilon}\right) + C + \frac{2\pi(x)}{\kappa}\sin^2\left(\frac{\pi}{2}\frac{y}{\delta}\right) && \text{Wall-Wake Law} \\ y^+ &= u^+ && \text{laminar sublayer} \end{aligned}\right\} \qquad (73)$$

where

$$y^+ = \frac{yu_\tau}{\upsilon}\,, \quad u^+ = \frac{u}{u_\tau} \qquad u_\tau = \sqrt{\tau_w/\rho}$$

and $\pi(x)/\kappa$ is evaluated from the condition that $u = u_\infty$ at $y/\delta = 1$. In Eq. (73) the constants κ and C are set at .41 and 5.0 respectively. This leaves two free parameters, τ_w (or C_f) and δ, which must be chosen to completely specify the profile. In (Ref. 34) tabulated values of C_f and δ are given, which are evaluated from curve fits of the experimental data as a function of streamwise position. The values corresponding to x = .6135 ft are

$$C_f = .004138$$

$$\delta = .015472 \text{ ft.}$$

Once the streamwise velocity profiles are obtained the normal velocity can be determined by approximating $\partial u/\partial x$ and then integrating the continuity equation.

In the calculation procedure the flow was assumed incompressible and in the streamwise direction the boundary layer option was employed, i.e. streamwise diffusion terms were dropped and a backward difference approximation was used for the streamwise convective terms. In the direction normal to the wall both second order finite differences and the fourth order G/OCI schemes were exercised. The full form of the dissipation function is used in the evaluation of the turbulent viscosity since in this case it did not have any perverse behavior. In the Newman airfoil calculation to be discussed shortly, however, the use of the full dissipation function adversely influenced the behavior of the solution. The solutions were obtained by marching in time until a steady state was reached.

The second order and fourth order calculation required 42 and 43 iterations respectively to converge, where a convergence criterion of $\varepsilon=10^{-5}$ was employed and ε corresponds to the maximum change in a primary variable (u,v) over a range of time steps. The total run time for the fourth order G/OCI calculation was 35.28 sec on a CDC 7600 computer which reduces to .00063sec per grid point per time step.

The skin friction distribution, C_f as a function of distance along the plate is presented in Figure 1. A comparison between the experimental data and both computations shows good agreement over most of the plate, with the major discrepancy appearing near the upstream boundary. There are two reasons for this. First, there is an incompatibility between the inflow profiles (obtained indirectly from experimental data) and the velocity profiles downstream of the inflow plane, which are obtained by the numerical solution of the governing equations. There is no direct method of avoiding this inherent error other than refining the mesh in the streamwise and normal directions in the vicinity of the inflow plane. This would allow any errors that are generated at the boundary to damp out several grid points downstream. Another method that could be used relies on completing two computations; the first beginning upstream of the inflow plane and extending downstream of it, and the second, the one of interest, on the actual computational domain. In the second calculation for the inflow profiles, one uses the profiles computed from the first calculation at the corresponding x location. Although such a procedure is not always applicable, it was used successfully for the Newman Airfoil Case (described below).

The second cause of the discrepancy, and probably the more serious, was the lack of resolution of the velocity profile at the upstream plane. Recall, that the top boundary was prescribed at some fixed constant height for all streamwise locations. The extent of the normal distance is based upon the consideration that at the downstream boundary the velocity profile should be totally contained within the computational domain. As a result at the upstream boundary the "boundary layer" occupies a small portion of the entire normal extent, leading to a lack of resolution there. This problem can easily be remedied by introducing a y/δ transformation which accounts for boundary layer growth and assures equal resolution in the normal direction for all x locations. In view of the benefits of this type of transformation it is recommended that the computer code be modified to include a y/δ transformation on option.

Despite the shortcomings discussed above, the errors near the inflow boundary die out rapidly and for the remainder of the flow field computations are in excellent agreement with the data. The velocity profile at x = 11.44 ft. (of Figure 2), also shows that good agreement was obtained between the computations and experiment.

In Figure 1, the increased accuracy of the fourth order generalized OCI scheme is evident. However, there were qualitative differences between the second order and fourth order solutions. The streamwise velocity profiles obtained by second order finite differences were smooth throughout the entire boundary layer. In contrast to this behavior the fourth order generalized OCI solutions tended to have slight wiggles near the outer edge of the boundary layer even though in theory the generalized OCI scheme should not if certain inequality constraints are satisfied. Unfortunately, near the outer edge these conditions are violated allowing for the observed behavior. We believe that the wiggles are due in part to high order numerical differentiation of the turbulent viscosity which possesses a sharp knee in the wake region of the layer. It is well known that higher order derivatives of rapidly varying functions introduce noise, and it is this noise which we believe we are witnessing. Laminar flow calculations have demonstrated that oscillatory behavior is not exhibited near the outer edge even for very coarse meshes. It is, therefore, felt that in order to obtain turbulent solutions commensurate with laminar solutions additional investigations of 'smoothing' procedures for the turbulent viscosity should be undertaken, and appropriate grid distributions be considered.

As a final note, the computation of C_f is discussed. Second order finite differences employ a three-point second-order one sided difference. A comparable formula accurate to fourth-order requires a five-point one-sided difference. As a result of the grid transformation employed, the formula encompasses points relatively far from the wall, and hence the computed C_f will be in error. Instead, for the reported results in Figure 1, a three-point, one-sided formula was used which gives more accurate values than the five-point scheme. Such behavior is not uncommon in computing one-sided derivatives (cf. Ref. 36).

Newman Airfoil Case

The Newman airfoil flow (case 3500 - series 2, Ref. 34) is considered next. It is more interesting and more difficult than the flat plate case due to the adverse pressure gradient present which leads to flow separation near the trailing edge. Indeed, the only meaningful numerical results obtained were those computed by second-order finite differences. The fourth-order calculations computed on the same grid were inaccurate and exhibited excessive oscillations near the outer edge of the computational domain. An explanation is suggested for the observed behavior, and a discussion of the computed results is presented.

In the computations a 36 x 36 grid was employed. In the streamwise direction which extends from x = 2.958 ft. to x = 4.926 ft. the spacing was uniform, while in the normal direction which extends from the wall to a fixed outer edge at y = .35 ft., a Roberts type stretching was used. The stretching parameter was chosen so that at the inflow plane the first grid point would be located within the sublayer ($y^+ = 1.75$). The Reynolds number for the flow was 769,231 per foot.

Initial flow computations revealed that the results were sensitive to both the external velocity distribution and the upstream velocity profile. Differentiating the velocity data given in Ref. 34 directly for use in the computation of the pressure gradient was found to work best. Numerically differentiating analytical curve fits to the external velocity distribution introduced errors in the pressure gradient and were thus discarded. In order to eliminate incompatabilities caused by a mismatch in the inflow conditions and the numerical solution, a preliminary calculation was performed on a 21 x 36 grid in the domain $2.759 \leq x \leq 3.2$, and the computed profiles at x = 2.958 were used as upstream conditions for the primary calculation. Since the pressure gradient in the upstream region was mild, there was no difficulty in obtaining a converged calculation for the 21 x 36 grid (the calculation converged in 21 iterations). However, the "boundary layer" form of the dissipation function was used since with that form the solutions behaved better near the outer edge of the computational domain.

In Figure 3 the computed skin friction distribution is presented and compared to the experimental data. The agreement is good for most of the airfoil with the exception of the trailing edge region where the second-order calculation predicts separation upstream of the actual separation point. However, for the shape factor, $H = \delta^*/\theta$ (cf. Fig.4) the agreement between data and computations is not as good, with the numerical results underpredicting the data. A lower value of H signifies that δ^* is too small, θ is too large or a combination of the two. In any event, the lack of agreement in H means that the velocity profile shape is incorrect. Two effects were considered to account for

this discrepancy; lack of spatial resolution and turbulence modeling. As discussed in the previous section, the inability to account for boundary layer growth leads to a spatial resolution problem. This effect manifests itself particularly near the upstream boundary where the boundary layer is thinnest. Since the major discrepencies in this case lie near the downstream boundary, where the boundary layer is thickest, poor grid resolution caused by the lack of a y/δ transformation is not a predominant factor for the observed behavior. Of course, grid resolution could be a real concern, but only in how it affects the numerical scheme in resolving regions of large gradients, i.e. the knee in the viscosity profile. In order to investigate the effect of turbulence modeling, a series of calculations were performed using a modified version of Cebeci's turbulent boundary layer code (Ref. 37) which uses Keller's Box scheme. This code permitted us not only to investigate turbulence modeling effects, but afforded us with a means of comparing our computational procedure with a different method, and running a series of mesh refinement studies.

The modified Cebeci code was checked out by computing the Weighardt case. After successful completion of this calculation, the Newman Airfoil case was attempted. In running the Newman Airfoil anamolies appeared which were not present in the Weighardt case. The computed skin friction coefficient exhibited oscillations in the streamwise direction. Since the "mean" C_f curve compared well with our calculations for $x > 3.5$ ft. and since our intent was to investigate the effects of turbulence modeling and grid refinement, we did not pursue the anamolous behavior. Even though oscillation in C_f were observed, we believe that they do not invalidate the conclusions to be drawn. The calculations were performed with 36 points in the streamwise direction (matching our calculations), and either 36, 60 or 100 points in the normal direction, which was stretched by a logarithmic transformation. It is important to point out that these calculations were performed in similarity variables so that the growth of the boundary layer was taken into account.

The results of the Box Scheme calculations were rather surprising. For the calculations using either Cebeci's two layer mixing length model (Ref. 14) or McDonald's model, the C_f distribution varied insignificantly from our second-order finite difference solution shown in Figure 3. For the comparison, the oscillating part was neglected and a mean C_f curve was considered. Neither was there much improvement with the use of a finer mesh indicating that 36 point is probably sufficient to resolve the flow. The major differences between Cebeci's model and Equation 37 are that in Cebeci's model, the outer layer mixing length is proportional to δ^*, while in Equation 37 it is proportional to δ, and in the Van Driest damping Cebeci includes a term that accounts for the pressure gradient.

The effects of these differences were considered next. In order to investigate the effect of pressure gradient terms in the Van Driest damping, the correction term was included in McDonald's model (Eq. 37). The results of the calculation with 36 points in the normal direction revealed that there was a significant shift of the C_f curve upward toward the data, with much better agreement obtained with the data. However, the oscillation still persisted. Why that term did not have a similar effect in Cebeci's mixing length model we cannot answer, and therefore, we believe further investigation is warranted.

In comparing the shape factor, the H distribution exhibited different behavior. These results are shown in Figure 4 which presents H as a function of x. It is apparent that the calculations using Cebeci's mixing length give better agreement with the data. Since the skin friction distribution did not compare as well, the good agreement of the shape factor with data must be related to the overall shape of the velocity profile. Hence, the velocity profiles obtained from Cebeci's model and from Eq. 37 were compared with data at x = 4.509 ft., (cf Fig. 5) to discover how the turbulence model effects the shape and thus H. Although the profile using Cebeci's model fits the data more closely, the shape of the velocity profile appears to be in error. Therefore, the good agreement for H shown in Figure 4 may be fortuitous. Further investigations beyond the scope of the present effort would be necessary to draw additional conclusions.

The following conclusions can be drawn from the calculations employing the Box Scheme:

(a) Mesh resolution in the normal direction was not a significant factor in the observed results.

(b) Choice of turbulence model can have a significant effect on the solutions.

In view of the above, the inclusion of a one-equation and/or a two-equation turbulence model in the computer code is recommended in any future effort.

Until now, we have neglected to say anything about the fourth-order calculations. The results obtained for a 36 x 36 grid exaggerated the mild oscillations in the velocity profiles observed in the Weighardt case. The inequality constraints required for nonoscillatory behavior of the generalized OCI scheme were violated. In order to satisfy these constraint conditions, more grid points, better transformations or both are necessary. It is, therefore, recommended that further investigation be performed in this area.

Two-Dimensional Unsteady Flow

The unsteady flow case considered is that of a nonzero mean flow with a sinusoidal unsteady component superimposed upon it, i.e.

$$u_e(t) = u_0(1 + A\cos\omega t) \tag{74}$$

where u_0 is the mean flow velocity, A is the dimensionless amplitude of the periodic part and ω is the circular frequency. For the case of laminar flow over a flat plate, Lighthill (Ref. 38) obtained expressions for the skin friction coefficient in the limit of low and high reduced frequency.

$$\frac{C_f}{2}\sqrt{R_x} = \begin{cases} 0.332 + A(0.498\cos\omega t - 0.849\omega x/u_0 \sin\omega t) & \omega x/u_0 \ll 1 \\ 0.332 + A(\omega x/u_0)^{1/2}\cos(\omega t + \pi/4) & \omega x/u_0 \gg 1 \end{cases} \tag{75}$$

It is convenient in the flow analysis to calculate the phase angle between the external velocity and a boundary layer property (i.e. skin friction coefficient) as a function of streamwise location, $x = x_0$. The derivation of the phase angle is presented below.

Consider an unsteady flow with an external velocity field that is a function of x and t

$$u_e(x,t) = u_0(x)\,(1 + A\cos\omega t) \tag{76}$$

and which has associated with it a boundary layer property f(x,t). Denoting the average value of a function by a super bar ($\bar{}$), the average external velocity at point x_0 is defined as

$$\bar{u}(x_0) = \frac{1}{T}\int_{t_1}^{t_1+T} u_0(x_0,t)\,dt = \frac{1}{T}\int_{t_1}^{t_1+T}\left[u_0(x_0)\right]\left[1 + A\cos\omega t\right]dt \tag{77}$$

or

$$\bar{u}(x_0) = u_0(x_0) \tag{78}$$

where $T = 2\pi/\omega$ is the period of oscillation ant t_1 is a reference time from which averaging begins. Similarly, the average value of the function f becomes

$$\bar{f}(x_0) = \frac{1}{T}\int_{t_1}^{t_1+T} f(x_0,t)\,dt \tag{79}$$

Here we have tactly assumed that the flow has reached a pseudo-steady state and initial transients have died out. For the cases considered here, such a state is reached after one period so that $t_1 = T$.

The function $f(x,t)$ is now expressed as a periodic function with frequency ω, i.e.

$$f(x,t) = \bar{f}(x_0) + B\cos\left[\omega t + \phi(x_0)\right] \tag{80}$$

where $\phi(x_0)$ is the phase angle between u_e and f at point $x = x_0$.

In order to determine the phase angle, the following integrals are evaluated

$$\cos\left[\phi(x_0)\right] = \frac{\frac{2}{T}\int_{t_1}^{t_1+T}\left(u_e(x_0,t) - u_0(x_0)\right)\cdot\left(f(x_0,t) - f(x_0)\right)dt}{B\,A\,u_0(x_0)} \tag{81}$$

and

$$B^2 = \frac{2}{T}\int_{t_1}^{t_1+T}\left(f(x_0,t) - \bar{f}(x_0)\right)^2 dt \tag{82}$$

The character of the flow field is governed in part by the amplitude of oscillation, A. Ackerberg and Phillips (Ref. 39) have shown that for A sufficiently small $A < .3$ no backflow will occur. However, for larger values, $A > .3$ regions of reverse flow will appear over the plate, predominantly near the downstream boundary. The occurrence of reverse flow at the downstream boundary has serious implications on the numerical solution of the governing equations, and will be discussed in greater detail below.

For the case considered in this report, A was chosen so as to avoid reverse flow from occurring, while the other input quantities were specified by numerical considerations (see below). Hence, the input data employed in the calculation are

$$u_o = .10$$

$$A = .125$$

$$\omega = 5\pi/2$$

$$X_U = .1$$

$$X_D = 3.6$$

$$Re = 666{,}667$$

Before describing the particulars of the calculations, a general discussion of the solution procedure, its features, and its associated constraints will be given. The solution procedure for the unsteady case follows along the same lines as for the steady case, with the essential difference being that in the unsteady case, the solution is advanced in real time with the time step chosen from considerations of temporal accuracy rather than rate of convergence. Whereas in the steady case, all boundary conditions are time invariant, for the oscillating flow the velocity distributions at the upstream and outer edge boundaries change with time. There is no difficulty in applying the outer edge velocity boundary condition since the velocity distribution is simply that which is given in Eq. (74). The upstream boundary is more troublesome. If the upstream boundary is located at $x = 0$, then at that point the boundary layer is of zero thickness and hence in transformed boundary layer coordinates remains fixed. In that case, the upstream inflow boundary condition remains Blasius independent of time. However, if the upstream boundary is located at some small, but finite, distance downstream of the leading edge, the velocity profile will change with time. Since the calculations were conducted in the physical plane rather than in the transformed plane, the upstream boundary was required to be placed at a small finite value of x. Hence, in order to account for the varying upstream boundary layer profile a method used by Singleton and Nash (Ref. 40) was employed, viz. the upstream boundary was scaled by the new edge velocity at each new time level. This procedure fixes the values of the flow variables at the upstream boundary, and permits the use of function conditions (necessary for well posedness) but as a result also introduces errors there.

By solving in the physical plane, boundary layer growth could not be very satisfactorily accounted for. This resulted in having the outer edge fixed at $y = 0.037$ ft.; the choice of this distance being predicated upon the necessity to accommodate the boundary layer at the downstream boundary. In Figure 6 the computed phase angle ϕ is presented and compared with Cebeci's calculations (Ref. 41), and to the low and high frequency predictions of Lighthill (Ref. 38). Both second-order and fourth-order calculations are shown, for $\beta = 1$. The agreement of our computations with the other predictions is very good for $\bar{\omega} \geq .8$. For small x there is a discrepancy due to the implementation of the upstream boundary condition described above, and the lack of a y/δ transformation. This effect was studied in greater detail at a lower frequency, $\omega = \pi/2$ and were compared to the calculations of Murphy (Ref. 42).

In Figure 7 second-order solutions with $\beta = 1$ and $\beta = 1/2$ (Crank Nicolson) are compared to Cebeci's results. The Crank Nicolson calculation gives larger values of ϕ than both the results for $\beta = 1$ and Ref. (41). Since Murphy's and Prenter's higher order calculations (Ref. 43) show the same trend, this would appear to indicate the improved accuracy of the Crank Nicolson scheme.

As A is increased, Phillips and Ackerberg (Ref. 39) show that reverse flow will occur during the cycle over some portion of the flat plate, including the downstream boundary. Although unsteady boundary layers permit regions of reverse flow, there is a difficulty in applying appropriate boundary conditions if at the downstream boundary fluid is entering the computational domain rather than exiting it. In an attempt to remedy this situation, Ackerberg and Phillips argue that since disturbances travel at some finite speed then at a distance sufficiently far downstream the flow will not have felt the disturbances generated at the leading edge and would, therefore, appear to be that which would exist on an infinite flat plate. The solution to that problem is well known, i.e. Rayleigh flow. Hence, they suggest that the Rayleigh solution be set at the downstream boundary (function condition) consistent with the corresponding x and t.

We investigated the behavior of our numerical scheme for a problem where reverse flow occurs, A = .3. The boundary conditions described in Ref. (39) were used for the solution of the full equations and central differences with artificial dissipation was employed in the streamwise direction. The calculations were run for two cycles, but the transients had not as yet died out completely. The results which we are not presenting at this time (since they are of a preliminary nature) indicate that there was no difficulty in the computations even when there were large regions of reverse flow. Future work will be aimed at conducting a more comprehensive study in this very important area. Additional effort will be extended on turbulent unsteady flows.

CONCLUSIONS

In this report we have presented results obtained by exploiting the computer code developed under a previous phase of the research effort to solve an approximate form of the time-dependent Navier-Stokes equations. Both two-dimensional turbulent and unsteady laminar cases are considered. The governing equations that are solved are more general than the conventional boundary layer equations, notably in the inclusion of streamwise and spanwise diffusion terms, although the pressure is still imposed by the external flow, as in conventional boundary layer theory. The computer code incorporates the split LBI scheme in conjunction with OR operator scheme that permits a variety of spatial difference schemes, including standard second-order finite differences, exponential type methods and fourth-order OCI techniques. In the split LBI scheme, an implicit sweep is performed in each spatial coordinate direction. A careful ordering of these sweeps permits an uncoupling of the continuity equation from the system in the first two implicit sweeps. Thus, on the first two sweeps the (tridiagonal) system block size is reduced from 3 x 3 to 2 x 2 with a resulting cost savings. On the last sweep of each time step all the equations in the system are linearly coupled and 3 x 3 blocks must be eliminated.

Results of computation indicate that the procedure is viable for more complex problems of interest. Higher order methods can yield more accurate results although care must be taken for turbulent flows when coarse grids are employed. For unsteady flows, the method is extremely efficient as a result of the noniterative nature of the algorithm. Future efforts will be aimed at incorporating a y/δ transformation, which will eliminate some of the difficulties encountered and will make the code more robust. Further investigations of appropriate turbulence models is also recommended with the one equation κ-ℓ model given priority.

ACKNOWLEDGEMENT

The authors would like to acknowledge the valuable assistance given by Dr. John Murphy in making available computer printouts of unsteady flow calculations conducted by him.

APPENDIX A

Linearization Technique

A number of techniques have been used for implicit solution of the following first-order nonlinear scalar equation in one dependent variable $\phi(x,t)$:

$$\partial\phi/\partial t = F(\phi)\,\partial G(\phi)/\partial x \tag{A1}$$

Special cases of Eq. (A1) include the conservation form if $F(\phi) = 1$, and quasi-linear flow if $G(\phi) = \phi$. Previous implicit methods for Eq. (A1) which employ nonlinear difference equations and also methods based on two-step predictor-corrector schemes are discussed by Ames (Ref. 44, p. 82) and von Rosenburg (Ref. 45), p. 56). One such method is to difference nonlinear terms directly at the implicit time level to obtain nonlinear implicit difference equations; these are then solved iteratively by a procedure such as Newton's method. Although otherwise attractive, there may be difficulty with convergence in the iterative solution of the nonlinear difference equations, and some efficiency is sacrificed by the need for iteration. An implicit predictor-corrector technique has been devised by Douglas and Jones (Ref. 46) which is applicable to the quasilinear case ($G = \phi$) of Eq. (A1). The first step of their procedure is to linearize the equation by evaluating the nonlinear coefficient as $F(\phi^n)$ and to predict values of $\phi^{n+1/2}$ using either the backward difference or the Crank-Nicolson scheme. Values for ϕ^{n+1} are then computed in a similar manner using $F(\phi^{n+1/2})$ and the Crank-Nicolson scheme. Gourlay and Morris (Ref. 47) have also proposed implicit predictor-corrector techniques which can be applied to Eq. (A1). In the conservative case ($F = 1$), their technique is to define $\hat{G}(\phi)$ by the relation $G(\phi) = \phi\hat{G}(\phi)$ when such a definition exists, and to evaluate $\hat{G}(\phi^{n+1})$ using values for ϕ^{n+1} computed by an explicit predictor scheme. With $\hat{G}$ thereby known at the implicit time level, the equation can be treated as linear and corrected values of ϕ^{n+1} are computed by the Crank-Nicolson scheme.

A technique is described here for deriving linear implicit difference approximations for nonlinear differential equations. The technique is based

on an expansion of nonlinear implicit terms about the solution at the known time level, t^n, and leads to a one-step, two-level scheme which, being linear in unknown (implicit) quantities, can be solved efficiently without iteration. This idea was applied by Richtmyer and Morton (Ref. 15, p. 203) to a scalar nonlinear diffusion equation. Here, the technique is developed for problems governed by ℓ nonlinear equations in ℓ dependent variables which are functions of time and space coordinates. The technique will be described for the three-dimensional, unsteady equations.

The solution domain is discretized by grid points having equal spacings in the computational coordinates, Δy^1, Δy^2 and Δy^3 in the y^1, y^2 and y^3 directions, respectively, and an arbitrary time step, Δt. The subscripts i, j, k and superscript n are grid point indices associated with y^1, y^2, y^3 and t, respectively, and thus $\phi^n_{i,j,k}$ denotes $\phi(y^1_i, y^2_j, y^3_k, t^n)$. It is assumed that the solution is known at the n level, t^n, and is desired at the (n+1) level, t^{n+1}. At the risk of an occasional ambiguity, one or more of the subscripts is frequently omitted, so that ϕ^n is equivalent to $\phi^n_{i,j,k}$.

The numerical method employed is quite general and is formally derived for systems of governing equations which have the following form:

$$\partial H(\phi)/\partial t = \mathcal{D}(\phi) + S(\phi) \qquad \text{(A2)}$$

where ϕ is a column vector containing ℓ dependent variables, H and S are column vector functions of ϕ, and $\mathcal{D}$ is a column vector whose elements are spatial differential operators which may be multidimensional. The generality of Eq. (A2) allows the method to be developed concisely and permits various extensions and modifications (e.g., noncartesian coordinate systems, turbulence models) to be made more or less routinely. It should be emphasized, however, that the Jacobian $\partial H/\partial\phi$ must usually be nonsingular if the ADI techniques as applied to Eq. (A2) are to be valid. A necessary condition is that each dependent variable appear in one or more of the governing equations as a time derivative. An exception would occur if for instance, a variable having no time derivative also appeared in only one equation, so that this equation could be decoupled from the remaining equations and solved a posteriori by an alternate method.

The linearized difference approximation is derived from the following implicit time-difference replacement of Eq. (A2):

$$(H^{n+1}-H^n)/\Delta t=\beta\left[\mathcal{D}(\phi^{n+1})+S^{n+1}\right]+(1-\beta)\left[\mathcal{D}(\phi^n)+S^n\right] \tag{A3}$$

where, for example, $H^{n+1} \equiv H(\phi^{n+1})$. The form of $\mathcal{D}$ and the spatial differencing are as yet unspecified. A parameter $\beta(0 \leq \beta \leq 1)$ has been introduced so as to permit a variable centering of the scheme in time. Equation (A3) produces a backward difference formulation for $\beta = 1$ and a Crank-Nicolson formulation for $\beta = 1/2$.

The linearization is performed by a two-step process of expansion about the known time level t^n and subsequent approximation of the quantity $(\partial\phi/\partial t)^n\Delta t$, which arises from chain rule differentiation, by $(\phi^{n+1} - \phi^n)$. The result is

$$H^{n+1} = H^n + (\partial H/\partial \phi)^n (\phi^{n+1}-\phi^n) + O(\Delta t)^2 \tag{A4a}$$

$$S^{n+1} = S^n + (\partial S/\partial \phi)^n (\phi^{n+1}-\phi^n) + O(\Delta t)^2 \tag{A4b}$$

$$\mathcal{D}(\phi^{n+1}) = \mathcal{D}(\phi^n) + (\partial \mathcal{D}/\partial \phi)^n(\phi^{n+1}-\phi^n) + O(\Delta t)^2 \tag{A4c}$$

The matrices $\partial H/\partial\phi$ and $\partial S/\partial\phi$ are standard Jacobians whose elements are defined, for example, by $(\partial H/\partial\phi)_{qr} \equiv \partial H_q/\partial\phi_r$. The operator elements of the matrix $\partial\mathcal{D}/\partial\phi$ are similarly ordered, i.e., $(\partial\mathcal{D}/\partial\phi)_{qr} \equiv \partial\mathcal{D}_q/\partial\phi_r$; however, the intended meaning of the operator elements requires some clarification. For the q^{th} row, the operation $(\partial\mathcal{D}_q/\partial\phi)^n(\phi^{n+1} - \phi^n)$ is understood to mean that $\{\partial/\partial t\,\mathcal{D}_q[\phi(x,y,z,t)]\}^n\Delta t$ is computed and that all occurrences of $(\partial\phi_r/\partial t)^n$ arising from chain rule differentiation are replaced by $(\phi_r^{n+1} - \phi_r^n)/\Delta t$.

After linearization as in Eqs. (A4), Eq. (A3) becomes the following linear implicit time-differenced scheme:

$$(\partial H^n/\partial\phi)(\phi^{n+1}-\phi^n)/\Delta t = \mathcal{D}(\phi^n)+S^n + \beta\,(\partial\mathcal{D}/\partial\phi + \partial S^n/\partial\phi)(\phi^{n+1}-\phi^n) \quad \text{(A5)}$$

Although H^{n+1} is linearized to second order in Eq. (A4), the division by Δt in Eq. (A3) introduces an error term of order Δt. A technique for maintaining formal second-order accuracy in the presence of nonlinear time derivatives is discussed by McDonald and Briley (Ref. 8), however, a three-level scheme results. Second-order temporal accuracy can also be obtained (for $\beta = 1/2$) by a change in dependent variable to $\hat{\phi} \equiv H(\phi)$, provided this is convenient, since the nonlinear time derivative is then eliminated. The temporal accuracy is independent of the spatial accuracy.

On examination, it can be seen that Eq. (A5) is linear in the quantity $(\phi^{n+1} - \phi^n)$ and that all other quantities are either known or evaluated at the n level. Computationally, it is convenient to solve Eq. (A5) for $(\phi^{n+1} - \phi^n)$ rather than ϕ^{n+1}. This both simplifies Eq. (A5) and reduces roundoff errors, since it is presumably better to compute a small $O(\Delta t)$ change in an $O(1)$ quantity than the quantity itself. To simplify the notation, a new dependent variable ψ defined by

$$\psi \equiv \phi - \phi^n \quad \text{(A6)}$$

is introduced, and thus $\psi^{n+1} = \phi^{n+1} - \phi^n$, and $\psi^n = 0$. It is also convenient to rewrite Eq. (A5) in the following simplified form:

$$(A + \Delta t\,\mathcal{L})\,\psi^{n+1} = \Delta t\left[\mathcal{D}(\phi^n)+S^n\right] \quad \text{(A7a)}$$

where the following symbols have been introduced to simplify the notation:

$$A \equiv \partial H^n/\partial\phi - \beta\Delta t\,(\partial S^n/\partial\phi) \quad \text{(A7b)}$$

$$\mathcal{L} \equiv -\beta(\partial\mathcal{D}/\partial\phi) \quad \text{(A7c)}$$

It is noted that $\mathcal{L}(\psi)$ is a linear transformation and thus $\mathcal{L}(0) = 0$. Furthermore if $\mathcal{L}(\phi)$ is linear, then $\mathcal{L}(\psi) = -\mathcal{L}\mathcal{D}(\psi)$.

Spatial differencing of Eq. (A7a) is accomplished simply by replacing derivative operators such as $\partial/\partial y^i$, $\partial^2/\partial y^i \partial y^i$ by corresponding finite difference operators, D_i, D_i^2. Henceforth, it is assumed that $\mathcal{D}$ and $\mathcal{L}$ have been discretized in this manner, unless otherwise noted.

Before proceeding, some general observations seem appropriate. The foregoing linearization technique assumes only Taylor expandability, an assumption already implicit in the use of a finite difference method. The governing equations and boundary conditions are addressed directly as a system of coupled nonlinear equations which collectively determine the solution. The approach thus seems more natural than that of making ad hoc linearization and decoupling approximations, as is often done in applying implicit schemes to coupled and/or nonlinear partial differential equations. With the present approach, it is not necessary to associate each governing equation and boundary condition with a particular dependent variable and then to identify various "nonlinear coefficients" and "coupling terms" which must then be treated by lagging, predictor-corrector techniques, or iteration. The Taylor expansion procedure is analogous to that used in the generalized Newton-Raphson or quasi-linearization methods for iterative solution of nonlinear systems by expansion about a known current guess at the solution (e.g., Bellman & Kalaba, Ref. 48). However, the concept of expanding about the previous time level apparently had not been employed to produce a noniterative implicit time-dependent scheme for coupled equations, wherein nonlinear terms are approximated to a level of accuracy commensurate with that of the time differencing. The linearization technique also permits the implicit treatment of coupled nonlinear boundary conditions, such as stagnation pressure and enthalpy at subsonic inlet boundaries, and in practice, this latter feature was found to be crucial to the stability of the overall method (Ref. 49).

APPENDIX B

GEOMETRIC PROPERTIES OF AIRFOILS

In this section we consider the vector properties of curves lying on a surface and relate them to their tensor equivalents. In particular a NACA four-digit airfoil section is considered, and its geometric properties are computed in vector and tensor form.

BASIC CONCEPTS

Consider a radius vector $\vec{r}$ drawn from an inertial reference frame 0 to a point P lying on a surface $\vec{S}$ (cf. Figure B-1). The tangent vector to the curve on the surface passing through P in the x_i direction is given by

$$\vec{e}_i = \frac{\partial \vec{r}}{\partial x_i} \tag{B-1}$$

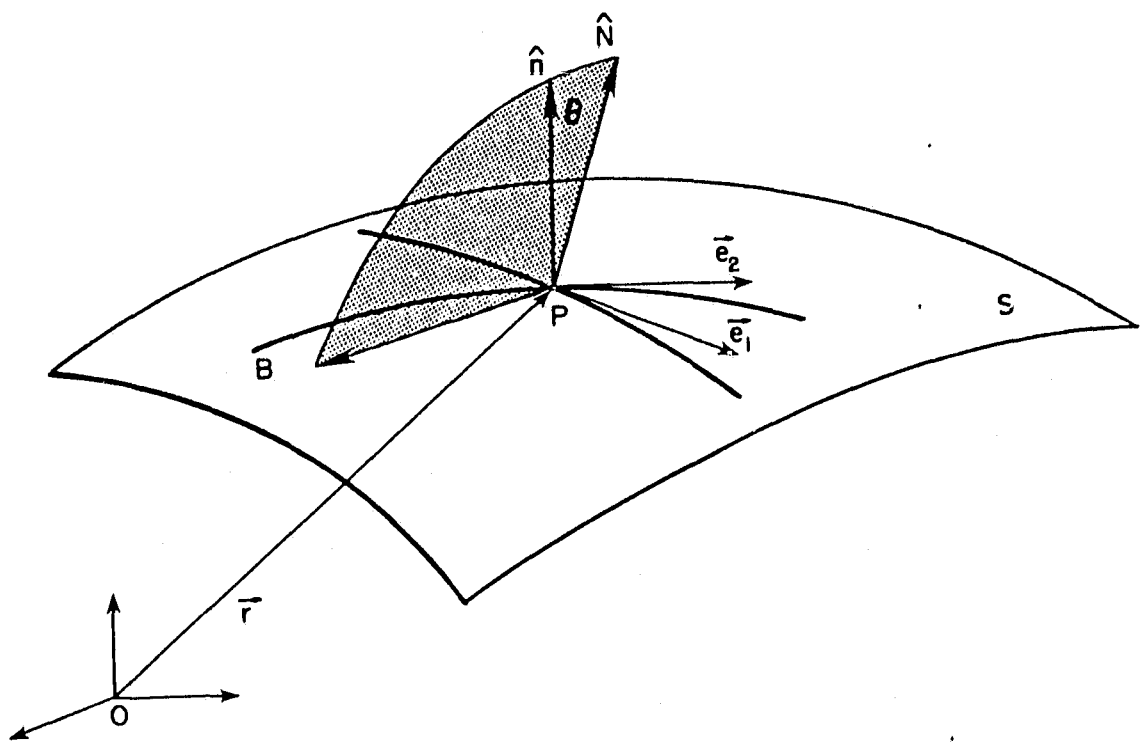

Figure B-1

The unit tangent vector is

$$\hat{t}_i = \frac{\partial \vec{r}}{\partial s_i} \tag{B-2}$$

where s_i is the arc length in the x_i direction. But from the chain rule, we obtain

$$\frac{\partial \vec{r}}{\partial x_i} = \frac{\partial \vec{r}}{\partial s_i}\frac{\partial s_i}{\partial x_i} = \hat{t}_i \frac{\partial s_i}{\partial x_i} = \vec{e}_i$$

By definition $\partial s_i/\partial x_i = h_i$, the metric, so that

$$\vec{t} = \frac{1}{h_i}\frac{\partial \vec{h}}{\partial x_i} \qquad \text{(no sum on i)} \tag{B-3}$$

The curve passing through point P in the direction $\vec{e}_i$ has a curvature $\vec{K}_i$ associated with it which is given as

$$\vec{K}_i = \frac{\partial \hat{t}_i}{\partial s_i} = \frac{\partial \hat{t}_i}{\partial x_i}\frac{\partial x_i}{\partial s_i} = \frac{1}{h_i}\frac{\partial \hat{t}_i}{\partial x_i}$$

$$= \frac{1}{h_i}\frac{\partial}{\partial r_i}\left(\frac{1}{h_i}\frac{\partial \vec{r}}{\partial x_i}\right) \tag{B-4}$$

$$\vec{K}_i = \frac{-1}{h_i^3}\frac{\partial h_i}{\partial x_i}\frac{\partial \vec{r}}{\partial x_i} + \frac{1}{h_i^2}\frac{\partial^2 \vec{r}}{\partial x_i^2}$$

The unit principal normal to the curve point at P is in the direction of $\vec{K}_i$ and denoted by $\hat{n}_i$, while the unit normal to the surface $\hat{N}$, at point P, is given by the cross product of the two tangent vectors at point P

$$\hat{t}_1 \times \hat{t}_2 = \hat{N} \sin\psi \tag{B-5}$$

where ψ is the angle between $\hat{t}_1$ and $\hat{t}_2$, i.e.

$$\cos\psi = \hat{t}_1 \cdot \hat{t}_2 = \frac{1}{h_1}\frac{\partial \vec{r}}{\partial x_1}\frac{1}{h_2}\frac{\partial \vec{r}}{\partial x_2}$$

so that

$$\sin\psi = \sqrt{1 - \cos^2\psi} = \frac{1}{h_1 h_2}\left[g_{11}g_{22} - g_{12}^2\right] \tag{B-6}$$

where g_{11}, g_{22} and g_{12} are the metric coefficients.

and

$$h_1 h_2 = \sqrt{g_{11} g_{22}}$$

The vector normal to both $\vec{e}_i$ and $\hat{N}$ is called the binormal, $\hat{B}_i$. Hence the curvature $\hat{K}_i$ can be represented by two components, one in the direction of $\hat{N}$, and one in the direction of $\vec{B}_i$ (cf. Figure B-2). These components are called the normal curvature K_n, and the geodesic curvature $\vec{K}_g$ respectively

$$K_n = \vec{K} \cdot \hat{N} = K \cos\theta$$

$$K_g = \vec{K} \cdot \vec{B} = K \sin\theta \qquad (7)$$

where θ is the angle between $\hat{n}$ and $\hat{N}$.

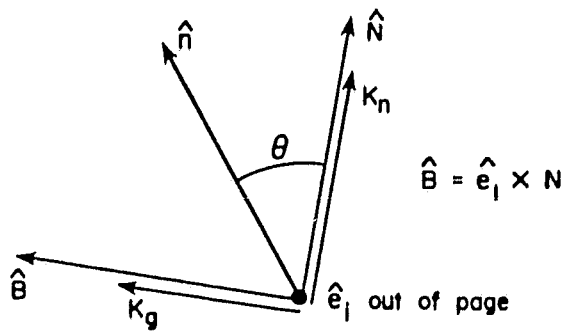

Figure B-2

DESCRIPTION OF NACA FOUR-DIGIT AIRFOIL

Consider an inertial reference frame in Cartesian coordinates

$$\bar{x}^i \equiv (\bar{x}1, \bar{x}^2, \bar{x}3) \text{ or equivalently } (\bar{x}, \bar{y}, \bar{z})$$

Attached to the airfoil is another Cartesian coordinate system given by

$$x^i = (x^1, x^2, x^3) \text{ or } (x, y, z)$$

(cf. Figure B-3).

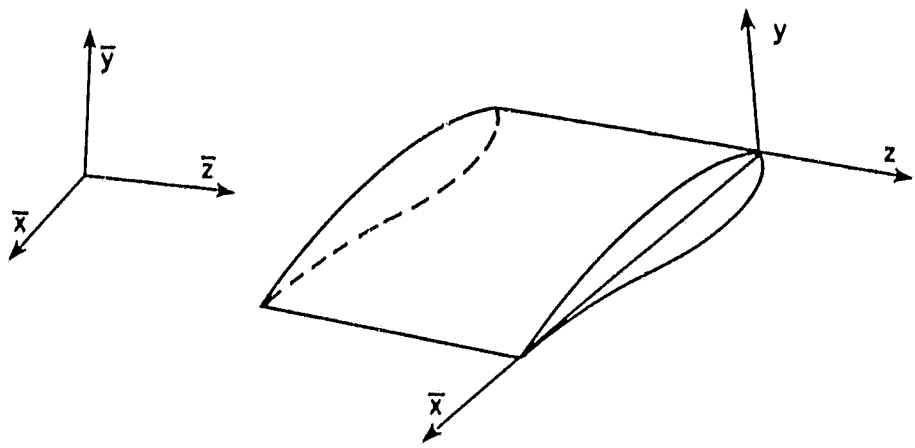

Figure B-3

The coordinate x is inclined at an angle α (the angle of attack) with respect to $\bar{x}$. In Figure 4 a two-dimensional airfoil is shown where Ⓛ and Ⓣ denote the leading and trailing edges, respectively.

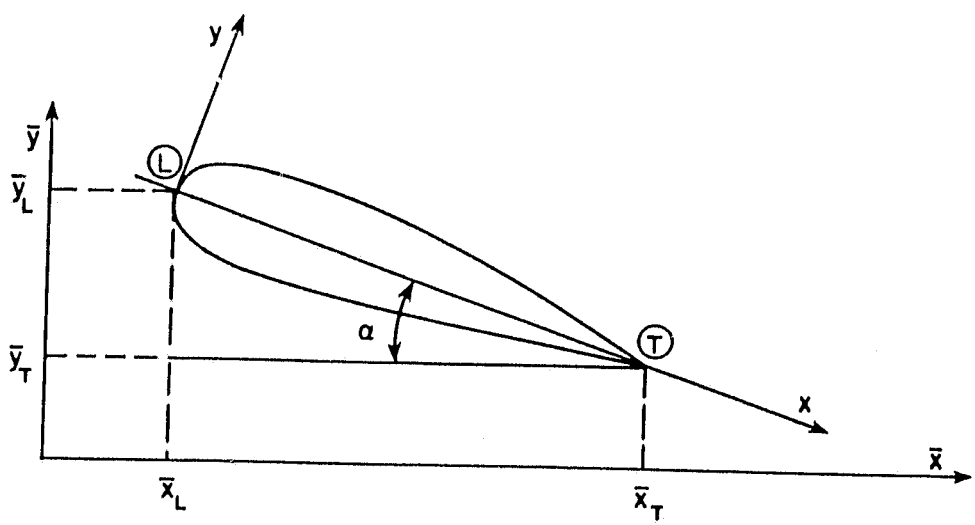

Figure B-4

The chord $\overline{LT}$ has length

$$c = ((x_T - x_L)^2 + (y_T - y_L)^2)^{1/2} \tag{B-8}$$

and in general can be a function of z the spanwise coordinate.

The thickness distribution for a NACA four-digit airfoil is given by

$$\pm \frac{y_t}{c} = \frac{t/c}{.20} \left\{ a_0 \sqrt{\tilde{x}} + a_1 \tilde{x} + a_2 \tilde{x}^2 + a_3 \tilde{x}^3 + a_4 \tilde{x}^4 \right\} \tag{B-9}$$

where $\tilde{x}=x/c$ (cf Ref. 50). For a cambered airfoil the thickness distribution is added onto the mean camber line. In the following, we will assume a symmetric uncambered airfoil with the mean line lying on the x axis.

Hence the designation of the airfoil which is considered is NACA 00XX, where XX refers to the thickness ratio t/c. In order to obtain a single valued $\tilde{y} = (y_t/c)$ function, the polar angle θ will be introduced (cf. Figure B-5).

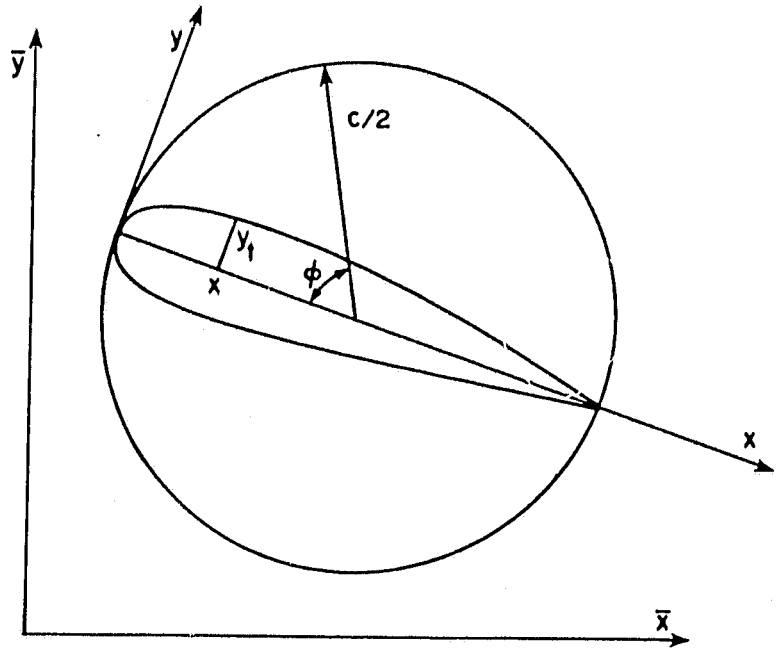

Figure B-5

The following relationships hold

$$x = -c/2 \cos\phi + c/2 = \frac{c}{2}(1 - \cos\phi)$$
$$\tilde{x} = -\frac{x}{c} = \frac{1}{2}(1 - \cos\phi) \qquad \text{(B-10)}$$

$\phi = 0$ leading edge $\qquad 0 \leq \phi \leq \pi$ upper surface

$\phi = \pi$ trailing edge $\qquad \pi \leq \phi \leq 2\pi$ lower surface

Hence, Equation (9) becomes

$$\frac{y_t}{c} = \tilde{y} = \frac{t/c}{.20}\tilde{g}(\phi) \qquad \text{(B-11)}$$

where $g(\phi)$ is the polar representation of the term in the brackets in Equation (B-9) and t and c can be functions of $\bar{z}$. Defining $g(\phi) = g(\phi)/.2$ and $\hat{t}(\bar{z}) = t(\bar{z})/c(\bar{z})$ y_t becomes

$$\tilde{y} = \hat{t}(\bar{z})\, g(\phi) \qquad \text{(B-12)}$$

The coordinate x can also be represented as a function of $\bar{z}$ and ϕ, i.e.

$$x = \frac{c(\bar{z})}{2}(1 - \cos\phi) = c(\bar{z})\, f(\phi)$$

and conversely ϕ can be represented as a function of x and $\bar{z}$

$$\phi = \cos^{-1}\left[1 - \frac{2\bar{x}}{c(\bar{z})}\right]$$

The relationship between the $(\bar{x},\bar{y})$ and (x,y) coordinate systems is

$$\frac{x}{c} = \frac{1}{c}\left\{(\bar{x} - \bar{x}_L)\cos\alpha - (\bar{y} - \bar{y}_L)\sin\alpha\right\}$$
$$\frac{y}{c} = \frac{1}{c}\left\{(\bar{x} - \bar{x}_L)\sin\alpha + (\bar{y} - \bar{y}_L)\cos\alpha\right\} \qquad \text{(B-13)}$$

alternatively

$$\frac{\bar{x}}{c} = \frac{1}{c}\left\{\bar{x}_L + x\cos\alpha + y\sin\alpha\right\}$$
$$\frac{\bar{y}}{c} = \frac{1}{c}\left\{\bar{y}_L + y\cos\alpha - x\sin\alpha\right\} \qquad \text{(B-14)}$$

Given a radius vector from the origin of the $(\bar{x},\bar{y},\bar{z})$ frame,

$$\vec{r} = \bar{x}\hat{i} + \bar{y}\hat{j} + \bar{z}\hat{k}$$

for the particular system under consideration

$$\begin{aligned} \bar{x} &= x_L + c(\bar{z})\, f(\phi)\cos\alpha + t(z)\, g(\phi)\sin\alpha \\ \bar{z} &= \bar{z} \\ \bar{y} &= \bar{y}_L + t(\bar{z})\, g(\phi)\cos\alpha - c(\bar{z})\, f(\phi)\sin\alpha \end{aligned} \tag{B-15}$$

Hence

$$\begin{aligned} \bar{x} &= \bar{x}(\bar{z}, \phi) \\ \bar{z} &= \bar{z} \\ \bar{y} &= \bar{y}(\bar{z}, \phi) \end{aligned} \tag{B-16}$$

and the surface coordinates will be lines of constant ϕ and constant $\bar{z}$.

In general on the surface we can write in symbolic form

$$\vec{r} = \bar{x}(\phi, \bar{z})\hat{i} + \bar{y}(\phi, \bar{z})\hat{j} + \bar{z}\hat{k} \tag{B-17}$$

The tangent vectors along the lines ϕ = constant and $\bar{z}$ = constant can be computed by differentiating the radius vector with respect to the coordinate line, i.e.

$$\vec{t}_1 = \frac{\partial \vec{r}}{\partial \phi} = \frac{\partial \bar{x}}{\partial \phi}\hat{i} + \frac{\partial \bar{y}}{\partial \phi}\hat{j}$$

$$\vec{t}_2 = \frac{\partial \vec{r}}{\partial \bar{z}} = \frac{\partial \bar{x}}{\partial \bar{z}}\hat{i} + \frac{\partial \bar{y}}{\partial \bar{z}}\hat{j} + \hat{k}$$

The unit tangent vectors are

$$\hat{t}_1 = \frac{\vec{t}_1}{|t_1|} = \frac{\bar{x}_\phi \hat{i} + \bar{y}_\phi \hat{j}}{\sqrt{\bar{x}_\phi^2 + \bar{y}_\phi^2}} \tag{B-18}$$

$$\hat{t}_2 = \frac{\vec{t}_2}{|t_2|} = \frac{\bar{x}_{\bar{z}} \hat{i} + \bar{y}_{\bar{z}} \hat{j} + \hat{k}}{\sqrt{1 + \bar{x}_{\bar{z}}^2 + \bar{y}_{\bar{z}}^2}} \tag{B-19}$$

The metric coefficients become

$$\begin{aligned} h_1^2 &= g_{11} = \bar{x}_\phi{}^2 + \bar{y}_\phi{}^2 \\ h_2^2 &= g_{22} = 1 + \bar{x}_z{}^2 + \bar{y}_{\bar{z}}{}^2 \end{aligned} \tag{B-20}$$

and

$$g_{12} = \bar{x}_\phi \bar{x}_{\bar{z}} + \bar{y}_\phi \bar{y}_{\bar{z}}$$

If $\hat{t}_1$ and $\hat{t}_2$ are orthogonal, $g_{12} \equiv 0$

The normal to the surface is obtained from the cross product of the surface unit tangent vectors

$$\hat{t}_1 \times \hat{t}_2 = \hat{N} \sin\psi$$

where ψ is the angle between $\hat{t}_1$ and $\hat{t}_2$.

In order to obtain $\sin\psi$, the dot product of the unit tangent vectors is employed

$$\hat{t}_1 \cdot \hat{t}_2 = \cos\psi$$

or

$$\frac{1}{h_2}\left[\bar{x}_{\bar{z}}\hat{i} + y_{\bar{z}}\hat{j} + \hat{k}\right] \cdot \frac{1}{h_1}\left[\bar{x}_\phi \hat{i} + \bar{y}_\phi \hat{j}\right] = \frac{1}{h_1 h_2}\left[\bar{x}_{\bar{z}} \cdot \bar{x}_\phi + \bar{y}_{\bar{z}}\, \bar{y}_\phi\right]$$

yielding the following relationship

$$\cos\psi = \frac{1}{h_1 h_2}\left[\bar{x}_{\bar{z}}\, \bar{x}_\phi + \bar{y}_{\bar{z}}\, \bar{y}_\phi\right]$$

Employing the expression

$$\sin\psi = \sqrt{1 - \cos^2\psi}$$

and with some algebraic manipulation the desired result is obtained.

$$\sin\psi = \frac{1}{h_1 h_2}\left\{g_{11}g_{12} - g_{12}^2\right\}^{1/2} \qquad \text{(B-21)}$$

In the case where ϕ and $\bar{z}$ are orthogonal to each other, $\psi = \pi/2$ and $g_{12} = 0$, or

$$\bar{x}_{\bar{z}}\, \bar{x}_\phi + \bar{y}_{\bar{z}}\, \bar{y}_\phi = 0$$

or

$$\bar{x}_{\bar{z}} = \bar{y}_{\bar{z}} = 0$$

The normal to the surface can now be computed

$$\hat{N} = \frac{1}{\sqrt{g_{11}g_{22} - g_{12}^2}}\left[-\bar{y}_\phi \hat{i} + \bar{x}_\phi \hat{j} - (\bar{x}_\phi \bar{y}_{\bar{z}} - \bar{y}_\phi\, \bar{x}_{\bar{z}})\hat{k}\right] \qquad \text{(B-22)}$$

From Equations (B-4) and (B-20), the curvature can be obtained in the ϕ direction (1 direction)

$$\vec{k}_1 = -\frac{1}{h_1^3}\frac{\partial h_1}{\partial \phi}\frac{\partial \vec{r}}{\partial \phi} + \frac{1}{h_1^2}\frac{\partial^2 \vec{r}}{\partial \phi^2} = -\frac{1}{h_1^3}\frac{\partial}{\partial \phi}\left[\bar{x}_\phi^2 + \bar{y}_\phi^2\right]^{1/2}\frac{\partial}{\partial \phi}\left[\bar{x}\hat{i} + \bar{y}\hat{j} + \bar{z}\hat{k}\right]$$

$$+ \frac{1}{h_1^2}\frac{\partial^2}{\partial \phi^2}\left[\bar{x}\hat{i} + \bar{y}\hat{j} + \bar{z}\hat{k}\right]$$

$$\vec{k}_1 = -\frac{1}{h_1^4}\left[\bar{x}_\phi \bar{x}_{\phi\phi} + \bar{y}_\phi \bar{y}_{\phi\phi}\right]\left[\bar{x}_\phi \hat{i} + \bar{y}_\phi \hat{j}\right] + \frac{1}{h_1^2}\left[\bar{x}_{\phi\phi}\hat{i} + \bar{y}_{\phi\phi}\hat{j}\right] \qquad \text{(B-23)}$$

Similarly K_2 is given as

$$\vec{k}_2 = -\frac{1}{h_2^3}\frac{\partial h_2}{\partial \bar{z}}\frac{\partial \vec{r}}{\partial \bar{z}} + \frac{1}{h_2^2}\frac{\partial^2 \vec{r}}{\partial z^2}$$

or

$$\vec{k}_2 = -\frac{1}{h_2^4}\left[\bar{x}_{\bar{z}}\bar{x}_{\bar{z}\bar{z}} + \bar{y}_{\bar{z}}\bar{y}_{\bar{z}\bar{z}}\right]\left[\bar{x}_{\bar{z}}\hat{i} + \bar{y}_{\bar{z}}\hat{j} + \hat{k}\right] + \frac{1}{h_2^2}\left[\bar{x}_{\bar{z}\bar{z}}\hat{i} + \bar{y}_{\bar{z}\bar{z}}\hat{j}\right] \qquad \text{(B-24)}$$

The geodesic curvatures can now be computed

$$K_{g_1} = \vec{K}_1 \cdot \vec{B}_1 = -\vec{K}_1 \cdot (\hat{t}_1 \times \hat{N})$$

where $\hat{t}_1$, $\hat{K}_1$ and $\hat{N}$ are given by Equations (B-18), (B-22), and (B-23).

After some algebra, we obtain

$$K_{g_1} = \frac{-1}{h_1^4 h_2 \sin\psi}(\bar{x}_\phi \bar{y}_{\phi\phi} - \bar{y}_\phi \bar{x}_{\phi\phi})(\bar{y}_{\bar{z}}\bar{x}_\phi - \bar{x}_{\bar{z}}\bar{y}_\phi) \qquad \text{(B-25)}$$

Similarly K_{g_2} becomes

$$K_{g_2} = \frac{1}{h_1^4 h_2^4 \sin\psi}\left[(\bar{x}_\phi \bar{y}_{\bar{z}} - \bar{y}_\phi \bar{x}_{\bar{z}})(\bar{y}_{\bar{z}}\bar{x}_{\bar{z}\bar{z}} - \bar{x}_{\bar{z}}\bar{y}_{\bar{z}\bar{z}}) + (\bar{x}_\phi \bar{x}_{\bar{z}\bar{z}} + \bar{y}_\phi \bar{y}_{\bar{z}\bar{z}})\right] \qquad \text{(B-26)}$$

We will now consider a NACA 4 digit airfoil and further assure X_L is a constant (non swept trailing edge). From Equation (15) we can obtain the appropriate derivatives

$$\begin{aligned}
\bar{x} &= x_L + c(\bar{z})\, f(\phi)\cos\alpha + t(\bar{z})\, g(\phi)\sin\alpha \\
\bar{x}_\phi &= c(\bar{x}) f_\phi \cos\alpha + t g_\phi \sin\alpha \\
\bar{x}_{\phi\phi} &= c\cos\alpha\, f_{\phi\phi} + t\sin\alpha g_{\phi\phi} \\
\bar{x}_{\bar{z}} &= c_{\bar{z}} f\cos\alpha + t_{\bar{z}} g\sin\alpha \\
\bar{x}_{\bar{z}\bar{z}} &= c_{\bar{z}\bar{z}} f\cos\alpha + t_{\bar{z}\bar{z}} g\sin\alpha
\end{aligned} \tag{B-27}$$

$$\begin{aligned}
\bar{y} &= \bar{y}_L + t(\bar{z})\, g(\phi)\cos\alpha - c(\bar{z})\, f(\phi)\sin\alpha \\
\bar{y}_\phi &= g_\phi t\cos\alpha - f_\phi c\sin\alpha \\
\bar{y}_{\phi\phi} &= g_{\phi\phi} t\cos\alpha - f_{\phi\phi} c\sin\alpha \\
\bar{y}_{\bar{z}} &= g\cos\alpha\, t_{\bar{z}} - f\sin\alpha c_{\bar{z}} \\
\bar{y}_{\bar{z}\bar{z}} &= g\cos\alpha t_{\bar{z}\bar{z}} - f\sin\alpha\, c_{\bar{z}\bar{z}}
\end{aligned} \tag{B-28}$$

For a rectangular plan form c and t are constant so that

$$\bar{x}_{\bar{z}} = \bar{x}_{\bar{z}\bar{z}} = 0$$

$$\bar{y}_{\bar{z}} = \bar{y}_{\bar{z}\bar{z}} = 0$$

Substituting Equations (B-27) and (B-28) into Equations (B-18) to (B-24) the appropriate geometric quantities can be obtained specialized for a NACA 00XX airfoil.

For the present code, the curvature terms are not used directly. Instead, the metric coefficients, g_{ij}, the Jacobian, J, and the Christoffel symbols, Γ^k_{ij} (cf Ref. 4) are used. These geometric functions are presented below.

Metric Coefficients:

$$\begin{aligned} g_{11} &= h_1^2 = \bar{x}_\phi^2 + \bar{y}_\phi^2 \\ g_{22} &= h_2^2 = \bar{x}_{\bar{z}}^2 + \bar{y}_{\bar{z}}^2 + 1 \\ g_{12} &= \bar{x}_\phi \bar{x}_{\bar{z}} + \bar{y}_\phi \bar{y}_{\bar{z}} \\ g_{33} &= 1 \\ J^2 &= \bar{x}_\phi^2 + \bar{y}_\phi^2 + \omega^2 \qquad \omega = \bar{x}_\phi \bar{y}_{\bar{z}} - \bar{y}_\phi \bar{x}_{\bar{z}} \end{aligned} \tag{B-29}$$

Basis vectors

$$\begin{aligned} \vec{e}_1 &= \bar{x}_\phi \hat{\imath} + \bar{y}_\phi \hat{\jmath} \\ \vec{e}_2 &= \bar{x}_{\bar{z}} \hat{\imath} + \bar{y}_{\bar{z}} \hat{\jmath} + \hat{k} \\ \vec{e}_3 &= \frac{1}{J} \left\{ -\bar{y}_\phi \hat{\imath} + \bar{x}_\phi \hat{\jmath} - \omega \hat{k} \right\} \end{aligned} \tag{B-30}$$

and

$$\hat{e}_1 = \vec{e}_1 / h_1 \ , \quad \hat{e}_2 = \vec{e}_2 / h_2 \ , \quad \hat{e}_3 = \vec{e}_3 \tag{B-31}$$

Christoffell Symbols (27 components)

$$\Gamma^3_{13} = \Gamma^3_{23} = \Gamma^3_{31} = \Gamma^3_{32} = 0$$

$$\Gamma^1_{33} = \Gamma^2_{33} = 0 \tag{B-32a}$$

$$\Gamma^3_{i3} = 0, \qquad i = 1, 2, 3$$

$$\Gamma_{11}^1 = \frac{1}{J^2}\left\{(\bar{x}_\phi \bar{x}_{\phi\phi} + \bar{y}_\phi \bar{y}_{\phi\phi}) + (\bar{y}_{\bar{z}} \bar{x}_{\phi\phi} - \bar{x}_{\bar{z}} \bar{y}_{\phi\phi})(\bar{x}_\phi \bar{y}_{\bar{z}} - \bar{x}_{\bar{z}} \bar{y}_\phi)\right\}$$

$$\Gamma_{12}^1 = \Gamma_{21}^1 = \frac{1}{J^2}\left\{\omega(\bar{y}_{\bar{z}} \bar{x}_{\phi\bar{z}} - \bar{y}_{\bar{z}} \bar{y}_{\phi\bar{z}}) + (\bar{x}_\phi \bar{x}_{\phi\bar{z}} + \bar{y}_\phi \bar{y}_{\phi\bar{z}})\right\}$$

$$\Gamma_{22}^1 = \frac{1}{J^2}\left\{(\bar{x}_\phi \bar{x}_{\bar{z}\bar{z}} + \bar{y}_\phi \bar{y}_{\bar{z}\bar{z}}) + (\bar{x}_\phi \bar{y}_{\bar{z}} - \bar{x}_{\bar{z}} \bar{y}_\phi)(\bar{y}_{\bar{z}} \bar{x}_{\bar{z}\bar{z}} - \bar{y}_{\bar{z}} \bar{y}_{\bar{z}\bar{z}})\right\}$$

$$\Gamma_{13}^1 = \Gamma_{31}^1 = \frac{1}{J^3}\left\{(\bar{y}_\phi \bar{x}_{\phi\phi} - \bar{x}_\phi \bar{y}_{\phi\phi}) + \left[\omega_\phi(\bar{x}_\phi \bar{x}_{\bar{z}} + \bar{y}_\phi \bar{y}_{\bar{z}}) - \omega(\bar{x}_{\bar{z}} \bar{x}_{\phi\phi} + \bar{y}_{\bar{z}} \bar{y}_{\phi\phi})\right]\right\}$$

$$\Gamma_{23}^1 = \Gamma_{32}^1 = \frac{1}{J^3}\left\{\left[\omega_{\bar{z}}(\bar{x}_\phi \bar{x}_{\bar{z}} + \bar{y}_\phi \bar{y}_{\bar{z}}) - \omega(\bar{y}_{\bar{z}} \bar{y}_\phi + \bar{x}_{\bar{z}} \bar{x}_{\phi\bar{z}})\right] + (\bar{y}_\phi \bar{x}_{\phi\bar{z}} - \bar{x}_\phi \bar{y}_{\phi\bar{z}})\right\}$$

$$\Gamma_{11}^2 = \frac{\omega}{J^2}(\bar{x}_\phi \bar{y}_{\phi\phi} - \bar{y}_\phi \bar{x}_{\phi\phi})$$

$$\Gamma_{12}^2 = \Gamma_{21}^2 = \frac{\omega}{J^2}(\bar{x}_\phi \bar{y}_{\phi\bar{z}} - \bar{y}_\phi \bar{x}_{\phi\bar{z}}) \qquad \text{(B-32b)}$$

$$\Gamma_{22}^2 = \frac{\omega}{J^2}(\bar{x}_\phi \bar{y}_{\bar{z}\bar{z}} - \bar{y}_\phi \bar{x}_{\bar{z}\bar{z}})$$

$$\Gamma_{13}^2 = \Gamma_{31}^2 = \frac{1}{J^3}\left\{\omega(\bar{y}_\phi \bar{y}_{\phi\phi} + \bar{x}_\phi \bar{x}_{\phi\phi}) - \omega_\phi(\bar{x}_\phi^2 + \bar{y}_\phi^2)\right\}$$

$$\Gamma_{23}^2 = \Gamma_{32}^2 = \frac{1}{J^3}\left\{\omega(\bar{x}_\phi \bar{x}_{\phi\bar{z}} - \bar{y}_\phi \bar{y}_{\phi\bar{z}}) - \omega_{\bar{z}}(\bar{x}_\phi^2 + \bar{y}_\phi^2)\right\}$$

$$\Gamma_{11}^3 = \frac{1}{J}(\bar{x}_\phi \bar{y}_{\phi\phi} - \bar{y}_\phi \bar{x}_{\phi\phi})$$

$$\Gamma_{12}^3 = \Gamma_{21}^3 = \frac{1}{J}(\bar{x}_\phi \bar{y}_{\phi\bar{z}} - \bar{y}_\phi \bar{x}_{\phi\bar{z}})$$

$$\Gamma_{22}^3 = \frac{1}{J}(\bar{x}_\phi \bar{x}_{\bar{z}\bar{z}} - \bar{y}_\phi \bar{y}_{\bar{z}\bar{z}})$$

These terms can be specialized for a NACA four digit airfoil by substituting Equations (B-27) and (B-28) into Equations (B-29) - (B-32).

APPENDIX C

Generalized Operator Compact Implicit Schemes

In this section a procedure for generating generalized OCI schemes is reviewed. Given

$$L(u) = u_{xx} + b(x)u_x + c(x)u$$

an expression relating L(u) and u is sought in the form

$$\frac{1}{h^2} RU_j = Q(Lu)_j + \tau_j \tag{C-1}$$

where τ_j is the truncation error and Q and R are tridiagonal displacement operators. The maximum accuracy attainable is fourth order, i.e., $\tau_j \sim O(h^4)$.

Expanding Eq. (20) in terms of $q_j^{-,c,+}$ and $r_j^{-,c,+}$ we obtain,

$$\begin{aligned}\tau_j = \frac{1}{h^2} RU_j - Q(Lu)_j = \frac{1}{h^2}\left[r_j^- U_{j-1} + r_j^c U_j + r_j^+ U_{j+1}\right] \\ - \left[q_j^-(Lu)_{j-1} + q_j^c(Lu)_j + q_j^+(Lu)_{j+1}\right]\end{aligned} \tag{C-2}$$

A Taylor series expansion yields for τ_j

$$\begin{aligned}\tau_j = T_j^0 u(x_j) + T_j^1 u^{(1)}(x_j) + T_j^2 u^{(2)}(x_j) + T_j^3 u^{(3)}(x_j) \\ + T_j^4 u^{(4)}(x_j) + T_j^5 u^{(5)}(x_j) + T_j^6 u^{(6)}(x_j) + O(h^5)\end{aligned} \tag{C-3}$$

where superscripts in parentheses denote derivatives with respect to x, and where

$$T_j^0 = \frac{1}{h^2}\left[(r_j^- + r_j^c + r_j^+) + h^2(q_j^- c_{j-1} + q_j^c c_j + q_j^+ c_{j+1})\right]$$

$$T_j^1 = \frac{1}{h}\left[(r_j^+ - r_j^-) - h(q_j^- b_{j-1} + q_j^c b_j + q_j^+ b_{j+1}) - h^2(q_j^+ c_{j+1} - q_j^- c_{j-1})\right]$$

$$T_j^2 = \frac{1}{2}(r_j^+ + r_j^-) - (q_j^- + q_j^c + q_j^+) \qquad \text{(C-4)}$$
$$- h(q_j^+ b_{j+1} - q_j^- b_{j-1}) - \frac{h^2}{2}(q_j^+ c_{j+1} + q_j^- c_{j-1})$$

$$T_j^\nu = h^{\nu-2}\left\{\frac{1}{\nu!}(r_j^+ + (-1)^\nu r_j^-) - \frac{h}{(\nu-1)!}(q_j^+ b_{j+1} + (-1)^{\nu-1} q_j^- b_{j-1})\right.$$
$$\left. - \frac{1}{(\nu-2)!}(q_j^+ + (-1)^\nu q_j^-) + h^2(q_j^+ c_{j+1} + (-1)^\nu q_j^- c_{j-1})\right\} \quad \nu = 3,4,5,6$$

For second order central finite differences we set $T^0 = T^1 = T^2 = 0$. This yields, when $q_j^c = 1$ and $q_j^- = q_j^+ = 0$, the following relations

$$r_j^c = -(r_j^- + r_j^+) + h^2(q_j^- c_{j-1} + q_j^c c_j + q_j^+ c_{j+1})$$

$$r_j^+ - r_j^- = hb_j = Rc_j$$

$$r_j^+ + r_j^- = 2$$

which recovers Eq. (45), i.e.,

$$r_j^c = -2 + h^2 c_j$$

$$r_j^- = 1 - Rc_j/2$$

$$r_j^+ = 1 + Rc_j/2$$

To obtain the fourth order operator compact implicit scheme we again set $T^0 = T^1 = T^2 = 0$ to obtain three expressions for $r_j^{-,c,+}$ in terms of the $q_j^{-,c,+}$, (note that q^-, $q^+ \neq 0$ and q^c is not necessarily unity), i.e.,

$$r_j^c = -(r_j^+ + r_j^-) + h^2(q_j^- c_{j-1} + q_j^c c_j + q_j^+ c_{j+1}) \tag{C-5a}$$

$$r_j^+ - r_j^- = Rc_{j-1}q_j^- + Rc_j q_j^c + Rc_{j+1}q_j^+ + h^2(q_j^+ c_{j+1} + q_j^- c_{j-1}) \tag{C-5b}$$

$$r_j^+ + r_j^- = 2(q_j^- + q_j^c + q_j^+) + 2\left[Rc_{j+1}q_j^+ - Rc_{j-1}q_j^-\right] + h^2(q_j^+ c_{j+1} + q_j^- c_{j-1}) \tag{C-5c}$$

Now T^3 and T^4 must be set to evaluate $q_j^{-,c,+}$. The standard Swartz OCI method requires $T^3 = T^4 = 0$,

$$\frac{1}{6}(r^+ - r^-) - \frac{1}{2}\left[Rc_{j+1}q_j^+ + Rc_{j-1}q_j^-\right] - \left[q_j^+ - q_j^-\right] = 0 \\ - h^2(q_j^+ c_{j+1} - q_j^- c_{j-1}) \tag{C-5d}$$

$$\frac{1}{24}(r^+ + r^-) - \frac{1}{6}\left[Rc_{j+1}q_j^+ - Rc_{j-1}q_j^-\right] - \frac{1}{2}\left[q_j^+ + q_j^-\right] = 0 \\ - h^2(q_j^+ c_{j+1} + q_j^- c_{j-1}) \tag{C-5e}$$

and results in a leading truncation error of the form $(\tilde{A}u^{(5)} + \tilde{B}u^{(6)})h^4$. Substituting (C-5b) and (C-5c) into (C-5d) and (C-53) r_j^+ and r_j^- can be eliminated and a system of two equations in q_j^- and q_j^c with q_j^+ as a parameter is obtained. The parameter q_j^c is proportional to the determinant of the system. The values of $q_j^{-,c,+}$ and $r_j^{-,c,+}$ are presented in Table I.

As shown in Ref. 20 a cell Reynolds number stability condition exists for the Swartz OCI scheme, i.e., for $Rc \geq \sqrt{12}$ nonrealistic or oscillatory solutions will be obtained. In order to eliminate this restriction one can relax the conditions $T^3 = T^4 = 0$, and allow the coefficients of $u^{(3)}$ and $u^{(4)}$ to be of $O(h^4)$.

By expanding $q_j^{-,c,+}$ in a series in Rc

$$q^{-,c,+} = \sum_{m=0}^{3} \lambda_m^{-,c,+} Rc_j^m \tag{C-6}$$

12 parameters, $\lambda_m^{-,c,+}$ $m = 0, 1, 2, 3$, are introduced. The equations for $T^3 = O(h^4)$ and $T^4 = O(h^4)$ yield 5 linear relations, leaving at one's disposal "6 free" parameters plus a factor.

These parameters can be set according to some criteria that would yield certain desirable properties for the difference equations. The following constraints are prescribed

$$\begin{gathered} q_j^+ \geq 0,\ q_j^- > 0,\ q_j^c > 0 \\ q_j^c b_j \geq q_j^- b_{j-1} + q_j^+ b_{j+1} \\ r_j^+ > r_j^- \geq 0 \\ -r_j^c \geq r_j^+ + r_j^- \end{gathered} \tag{C-7}$$

and h is sufficiently small so that

$$10b_j - b_{j-1} - b_{j+1} > 0 \quad \text{and} \quad 2 + hc_{j+1}/b_{j+1} > 0$$
$$\text{for } j = 2, \cdots, J \text{ and } c_j \leq 0$$

These conditions assure that R is diagonally dominant and Q is invertible for all R_c. Further details are given in Ref. 27. The significance of this approach is that one can construct a scheme possessing certain desired properties by employing a set of preassigned rules. This is contrary to usual practice, in which a scheme is chosen, and then its properties are determined. Although the computational effort in computing the q and r coefficients is not cheap, the actual percentage of the total cost is minimal. This has been borne out in actual computations.

The q and r coefficients for the generalized OCI scheme described in Ref. 27 are given in Table II.

REFERENCES

1. Kendall, R.M., Bonnett, W.S., Nardo, C.T. and Abbett, M.J.: Computational Procedure for Three-Dimensional Boundary Layers on Aircraft and Aerospace Vehicles. Proceedings AIAA 2nd Fluid Dynamics Conference, Hartford, 1975, pp. 113-121.

2. Briley, W.R. and McDonald, H.: On the Structure and Use of Linearized Block ADI and Related Schemes. J. Comp. Physics, Vol. 34, No. 1, 1980.

3. Weinberg, B.C. and McDonald, H.: Solution of Three-Dimensional Time-Dependent Viscous Flows, Part 1: Investigation of Candidate Algorithms. SRA Report R79-90004, Final Contractor's Report,(NAS2-10016), 1979.

4. Weinberg, B.C. and McDonald, H.: Solution of Three-Dimensional Time-Dependent Viscous Flows, Part 2: Development of the Computer Code, Final Contractor's Report, (NAS2-10016), 1980.

5. Nash, J.F. and Patel, V.C.: Three-Dimensional Turbulent Boundary Layers. Scientific and Business Consultants Inc., 1972.

6. Lin, T.C. and Rubin, S.G.: Viscous Flow over a Cone at Moderate Incidence, Part 2. Supersonic Boundary Layer, J. Fluid Mech., Vol. 59, Part 3, 1973, pp. 593-620.

7. Briley, W.R.: Numerical Method for Predicting Three-Dimensional Steady Viscous Flow in Ducts. J. Comp. Physics, Vol. 14, No. 1, 1974.

8. McDonald, H. and Briley, W.R.: Three-Dimensional Supersonic Flow of a Viscous or Inviscid Gas. J. of Comp. Physics, Vol. 19, No. 2, 1975.

9. Blottner, F.G.: Investigation of Some Finite Difference Techniques for Solving the Boundary Layer Equations. Computer Methods in Applied Mechanics and Engineering. Vol. 6, 1975, pp. 1-30.

10. Howarth, L.: The Boundary Layer in Three-Dimensions-Part I. Derivation of the Equations for Flow Along a General Curved Surface. Philosophical Magazine, Vol. 7, 1951, pp. 239.

11. Roberts, G.O.: Computational Meshes for Boundary Layer Problems. Proceedings of the Second International Conference on Numerical Methods in Fluid Dynamics, Springer-Verlag, New York, 1971, p. 171.

12. Flugge, W.: Tensor Analysis and Continuum Mechanics, Springer-Verlag, 1972.

13. Eiseman, P.R.: The Numerical Solution of the Fluid Dynamical Equations in Curvilinear Coordinates. Air Force Weapons Laboratory Report AFWL-TR-73-172.

14. Cebeci, T., Kaups, K. and Ramsay, J.A.: A General Method for Calculating Three-Dimensional Compressible Laminar and Turbulent Boundary Layers on Arbitrary Wings, NASA CR-2777, January 1977.

15. Richtmyer, R.D. and Morton, K.W.: Difference Methods for Initial Value Problems. Second Edition. Interscience Publishers, New York, New York, 1967.

16. Favre, A.: Equations des Gaz Turbulents Compressibles. J. de Mecanique, Vol. 4, pp. 361-392, 1965.

17. Kreskovsky, J.P., Shamroth, S.J. and McDonald, H.: Application of a General Boundary Layer Analysis to Turbulent Boundary Layers Subjected to Strong Favorable Pressure Gradients, J. of Fluids Engineering, pp. 217-224, June 1975.

18. McDonald, H. and Camarata, F.J.: An Extended Mixing Length Approach for Computing the Turbulent Boundary Layer Development, Proceedings Computation of Turbulent Boundary Layers - 1968 AFOSR-IFP Stanford Conference, Vol. 1, pp. 83-98, 1969.

19. Douglas, J. and Gunn, J.E.: A General Formulation of Alternating Direction Methods. Numerische Math., Vol. 6, 1964, p. 428.

20. Berger, A.E., Solomon, J.M., Ciment, M., leventhal, S.H. and Weinberg, B.C.: Generalized OCI Schemes for Boundary Layer Problems, Math Comp., Vol. 35, No. 151, 1980.

21. Allen, D.N. and Southwell, R.V.: Relaxation Methods Applied to Determine the Motion, in Two Dimensions, of a Viscous Fluid Past a Fixed Cylinder, Quart. J. Mech. Appl. Math., 8, 1955, pp. 129-145.

22. Il'in, A.M.: Differencing Scheme for a Differential Equation with a Small Parameter Affecting the Highest Derivative. Mat. Zametki, 6, 1969, pp. 237-248 - Math. Notes, 6, 1969, pp. 596-602.

23. McDonald, H.: A Novel Finite Difference Scheme Particularly Suited for Fluid Flow Problems Containing Discontinuities. Scientific Research Associates Report P76-1, August 1976.

24. Dennis, S.C.R.: Finite Differences Associated with Second-Order Differential Equations, Quart. J. Mech. Appl. Math., Vol. 23, 1960, pp. 487-507.

25. El-Mistikawy, T.M. and Werle, M.J.: Numerical Methods for Inviscid, Viscous Fluid Flows, Report No. AFL 77-9-34, University of Cincinnati, March 1977.

26. El-Mistikawy, T.M., and Werle, M.J.: Numerical Method for Boundary Layers with Blowing - the Exponential Box Scheme. AIAA J., 16, 1978, pp. 749-751.

27. Berger, A.E., Solomon, J.M. and Ciment, M.: An Analysis of a Uniformly Accurate Finite Difference Method for a Singular Perturbation Problem. Paper presented at Second International Conference on Computational Methods in Nonlinear Mechanics. March 26-30, Austin, Texas.

28. Leventhal, S.J.: The Operator Compact Implicit Method for Reservoir Simulation, Proceedings of Fifth SPE Symposium on Numerical Resevoir Simulation, 1979.

29. Blottner, F.G.: Computational Techniques for Boundary Layers in "Computational Methods for Inviscid and Viscous Two and Three-Dimensional Flow Fields". Fluid Dynamics Institute, Hanover, New Hmapshire, 1975.

30. Weinberg, B.C., Leventhal, S.H. and Ciment, M.: The Operator Compact Implicit Scheme for Viscous Flow Problems. AIAA Paper No. 77-638. Presented at the 3rd AIAA Comp. Fluid Dynamics Conf., Albuquerque, N.M., 1977.

31. Weinberg, B.C.: Viscous Flow Calculations Employing a Fourth Order Generalized Operator Compact Implicit Scheme, Paper 79-1468, Presented at 4th AIAA Comp. Fluid Dynamics Conf., Williamsburg, Va., 1979.

32. Gibeling, H.J., Shamroth, S.J. and Eiseman, P.R.: Analysis of Stong-Interaction Dynamic Stall for Laminar Flow on Airfoils. NASA CR-2969, April 1978.

33. Fairweather, G. and Mitchell, A.K.: A New Computational Procedure for ADI Methods, SIAM J. Numer. Anal., Vol. 4, No. 2, 1967.

34. Coles, D.E. and Hirst, E.A. (Editors): Proceedings Computation of Turbulent Boundary Layers - 1968. AFOSR-IFP Stanford Conference, Vol. I, Compiled Data, 1969.

35. Oh, Y.H.: An Analytical Transformation Technique for Generating Uniformly Spaced Computational Mesh. Old Dominion University Research Foundation, October 1978.

36. Carnahan, B., Luther, H.A. and Wilkes, J.O.: Applied Numerical Methods," John Wiley & Sons, pp. 130, 1969.

37. Cebeci, T. & Bradshaw, P., "Momentum Transfer in Boundary Layers," Hemisphere Publishing Co., 1977, Chapter 8.

38. Lighthill, M.J., "The Response of Laminar Skin Friction and Heat Transfer to Fluctuations in the Stream Velocity," Proc. Roy. Soc. 224A p. 1-23, 1954.

39. Phillips, J.H., and Ackerberg, R.C., "A Numerical Method for Integrating the Unsteady Boundary-Layer Equations When There are Regions of Back Flow," JFM Vol. 58, Part 3, pp. 561-579, 1973.

40. Singelton, R.E. and Nash, J.F.: A Method for Calculating Unsteady Turbulent Boundary Layers in Two and Three Dimensions, AIAA J., Vol. 12, No. 5, pp. 590-595, 1974.

41. Cebeci, T. and Carr, L.W.: A Computer Program for Calculating Laminar and Turbulent Boundary Layers for Two-Dimensional Time-Dependent Flows, NASA TM-78470, March 1978.

42. Murphy, J., private communication.

43. Murphy, J.D. and Prenter, P.M., "A Hybrid Computing Scheme for Unsteady Turbulent Boundary Layers," 3rd Symposium Shear Flows, 1981, pp. 8.26, 8.34.

44. Ames, W.F.: Numerical Methods for Partial Differential Equations. Barnes & Noble, Inc., New York, New York, 1969.

45. von Rosenberg, D.A.: Methods for the Numerical Solution of Partial Differential Equations. American Elsevier Publishing Co., Inc., New York, New York, 1969.

46. Douglas, J., and Jones, B.F.: On Predictor-Corrector Methods for Nonlinear Parabolic Differential Equations. Soc. for Indust. Appl. Math., Vol. 11, 1963, pp. 195-204.

47. Gourlay, A.R., and Morris, J.L.: Finite-Difference Methods for Nonlinear Hyperbolic Systems. Math. Comp., Vol. 22, 1968, pp. 28-39.

48. Bellman, R.E., and Kalaba, R.E.: Quasilinearization and Nonlinear Boundary-Value Problems. American Elsevier Publ. Co., Inc., New York, 1965.

49. Briley, W.R., and McDonald, H.: Solution of the Multidimensional Compressible Navier-Stokes Equations by a Generalized Implicit Method. J. Comp. Physics, Vol. 24, No. 4, August, 1977, p. 372.

50. Abbot, I.H., and VonDoenhoff, A.E.: Theory of Wing Sections, Dover Publishing Co., 1959.

TABLE I. - OPERATOR COEFFICIENTS FOR STANDARD OPERATOR COMPACT IMPLICIT SCHEME

$$q_j^- = 6 - 5\rho_j + 2\rho_{j+1} - \rho_j\rho_{j+1}$$

$$q_j^c = 60 + 16\rho_{j+1} - 16\rho_{j-1} - 4\rho_{j-1}\rho_{j+1}$$

$$q_j^+ = 6 + 5\rho_j - 2\rho_{j-1} - \rho_j\rho_{j-1}$$

$$r_j^- = q_j^-\left(1 - \frac{3}{2}\rho_{j-1}\right) + q_j^c\left(1 - \frac{1}{2}\rho_j\right) + q_j^+\left(1 + \frac{1}{2}\rho_{j+1}\right) + h^2 q_j^- c_{j-1}$$

$$r_j^c = -(r_j^+ + r_j^-) + h^2(q_j^- c_{j-1} + q_j^c c_j + q_j^+ c_{j+1})$$

$$r_j^+ = q_j^-\left(1 - \frac{1}{2}\rho_{j-1}\right) + q_j^c\left(1 + \frac{1}{2}\rho_j\right) + q_j^+\left(1 + \frac{3}{2}\rho_{j+1}\right) + h^2 q_j^+ c_{j+1}$$

where

$$\rho_j = hb_j$$

TABLE II. - OPERATOR COEFFICIENTS FOR GENERALIZED OPERATOR COMPACT IMPLICIT SCHEME

$$q_j^- = 6 + [p_1 - 3]Rc_j + [p_2]Rc_j^2$$

$$q_j^c = 60 + [10p_1]Rc_j + [p_3]Rc_j^2 + [\tau_{j+1}p_4]Rc_j^3$$

$$q_j^+ = 6 + [p_1 + 3]Rc_j + [p_1 + p_2]Rc_j^2 + [p_4]Rc_j^3$$

where

$$p_1 = 3 \ , \ p_2 = 0 \ , \ p_3 = \max[\pi_1, \pi_2]$$

$$\pi_1 = (\tau_{j+1} + \tau_{j-1})p_2 + \tau_{j+1}p_1 + \bar{\pi}_1 \qquad \pi_2 = 15 - 2p_2 + (\sigma_2 - 1)p_1 - 3(\tau_{j+1} + \sigma_2) + \bar{\pi}_2$$

$$\bar{\pi}_1 = \begin{cases} 0 & \sigma_1 \geq 0 \\ \frac{3}{8}\sigma_1^2(10 - \tau_{j+1} - \tau_{j-1}) & \sigma_1 \leq 0 \end{cases} \qquad \bar{\pi}_2 = \begin{cases} 0 & 2p_1 - \sigma_2 \geq 0 \\ (2p_1 - \sigma_2)^2/8 & 2p_1 - \sigma_2 < 0 \end{cases}$$

$$\sigma_1 = p_1/3 + \frac{(\tau_{j-1} - \tau_{j+1})}{10 - \tau_{j+1} - \tau_{j-1}} \qquad 2\sigma_2 = 3\tau_{j-1} - \tau_{j+1} + 10 + 2h\tau_{j-1}\left(\frac{c_{j-1}}{b_{j-1}}\right)$$

$$p_4 = \frac{1}{2}\left[1 + \tau_{j+1}\right]^{-1}\pi_3 \qquad \pi_3 = p_3 - \pi_1 + \bar{\pi}_1 + 2\tau_{j-1}\left(2 + h\frac{c_{j-1}}{b_{j-1}}\right)p_2$$

with h sufficiently small so that

$$10b_j - b_{j-1} - b_{j+1} > 0 \text{ and } 2 + hc_{j+1}/b_{j+1} > 0 \text{ for } j = 2, \cdots, J \text{ and } c_j \leq 0$$

where

$$\tau_{j-1} = b_{j-1}/b_j \ , \ \tau_{j+1} = b_{j+1}/b_j \text{ and } Rc_j = hb_j$$

r_j^-, r_j^c, r_j^+ given in TABLE I

TABLE III.- OPERATOR COEFFICIENTS FOR
ALLEN SOUTHWELL EXPONENTIAL SCHEME

$$r_j^- = Rc_j\, e^{-Rc_j} \Big/ (1 - e^{-Rc_j})$$

$$r_j^+ = Rc_j \Big/ (1 - e^{-Rc_j})$$

$$r_j^c = -Rc_j + c_j$$

$$q_j^- = 0$$

$$q_j^c = 1$$

$$q_j^+ = 0$$

where $Rc_j = h b_j$

TABLE IV. - OPERATOR COEFFICIENTS FOR EL-MISTIKAWY WERLE EXPONENTIAL BOX SCHEME

$$r_j^- = \rho^- \exp(-\rho^-) \,/\, \left[1 - \exp(-\rho^-)\right]$$

$$r_j^+ = \rho^+ \,/\, \left[1 - \exp(-\rho^+)\right]$$

$$r_j^c = -(r_j^+ + r_j^-)$$

$$q_j^- = (1 - r_j^-) \,/\, (2\rho^-)$$

$$q_j^+ = (r_j^+ - 1) \,/\, (2\rho^+)$$

$$q_j^c = q_j^- + q_j^+$$

where

$$\rho^- = \frac{1}{2}(\rho_{j-1} + \rho_j) \quad , \quad \rho^+ = \frac{1}{2}(\rho_j + \rho_{j+1})$$

and

$$\rho_j = hb_j$$

TABLE V. - OPERATOR COEFFICIENTS FOR SECOND ORDER FINITE DIFFERENCES WITH ARTIFICIAL VISCOSITY

$$r_j^- = 1 - S$$

$$r_j^c = -2 + ct$$

$$r_j^+ = 1 + S$$

$$q_j^- = 0$$

$$q_j^c = t$$

$$q_j^+ = 0$$

where $S = Rc_{max}/2$ for $Rc_j > Rc_{max}$

$S = -Rc_{max}/2$ for $Rc_j < -Rc_{max}$

$$t = \frac{Rc_{max}}{|Rc_j|}$$

and $Rc_j = hb_j$

for $|Rc_j| < Rc_{max}$, r_j^-, r_j^c, r_j^+, q_j^-, q_j^c, q_j^+

reduce to standard finite differences.

where Rc_{max} is the maximum allowable cell Reynolds number

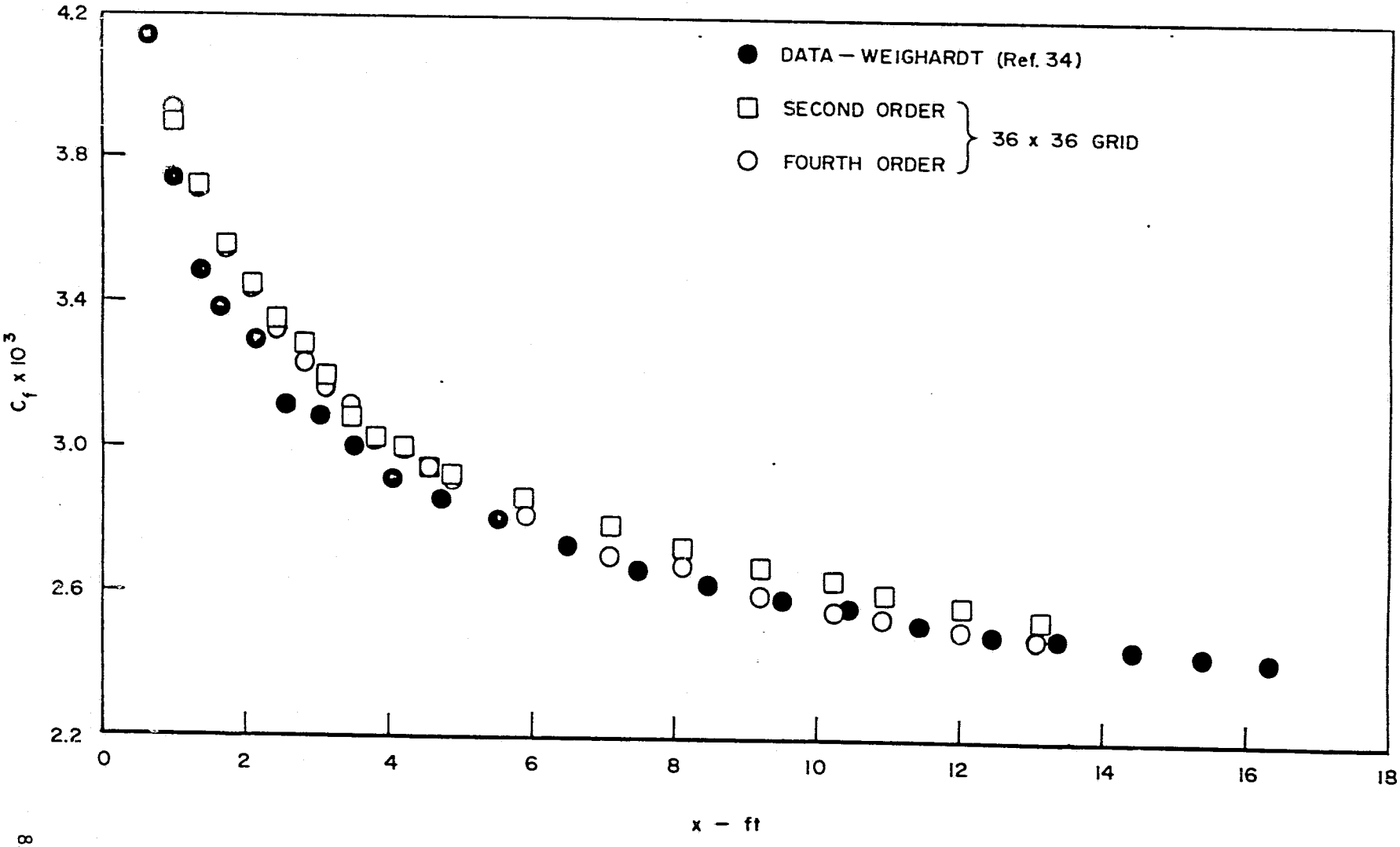

FIG I. SKIN FRACTION DISTRIBUTION AS A FUNCTION OF x

FIG. 2. VELOCITY PROFILE

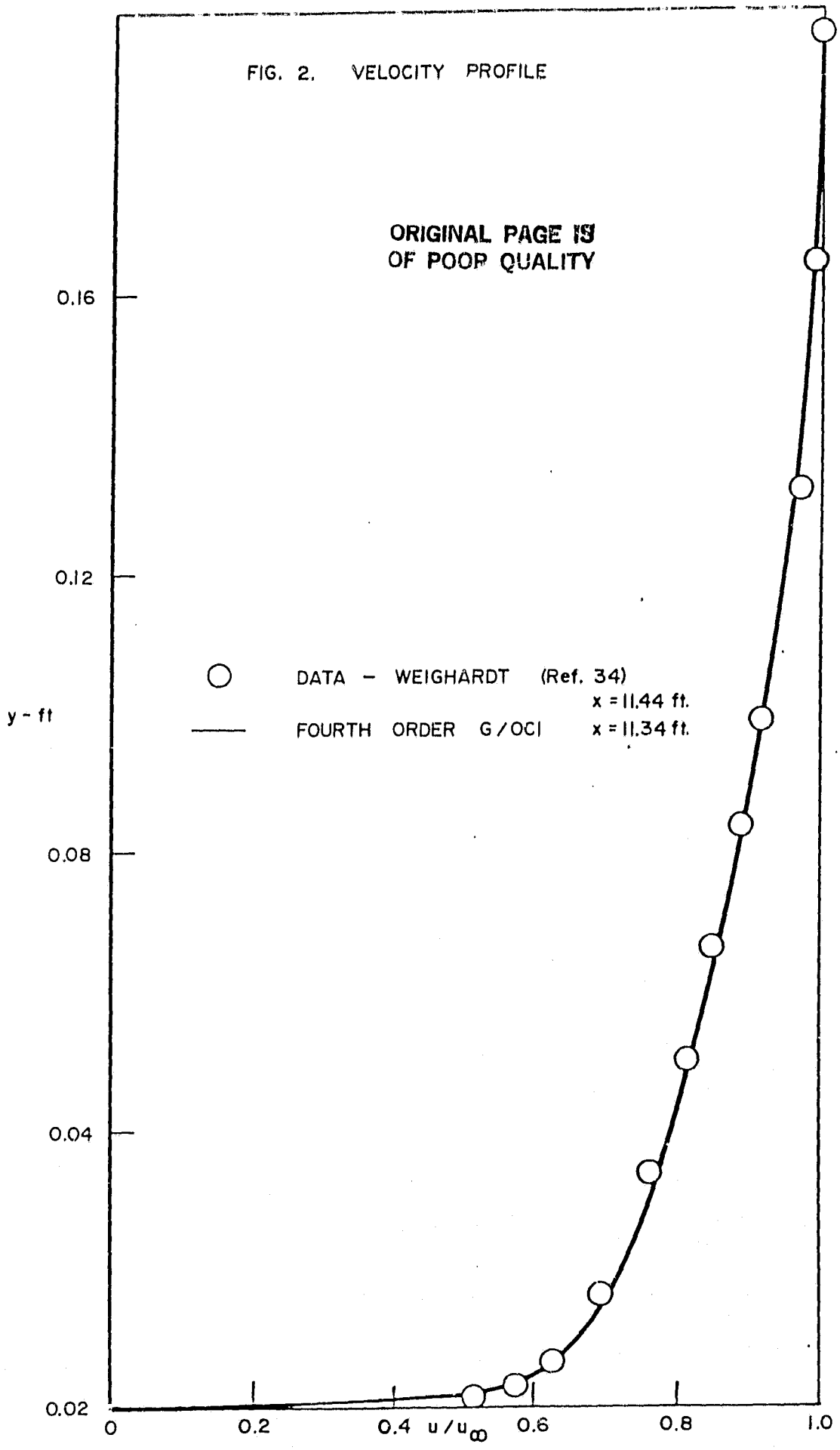

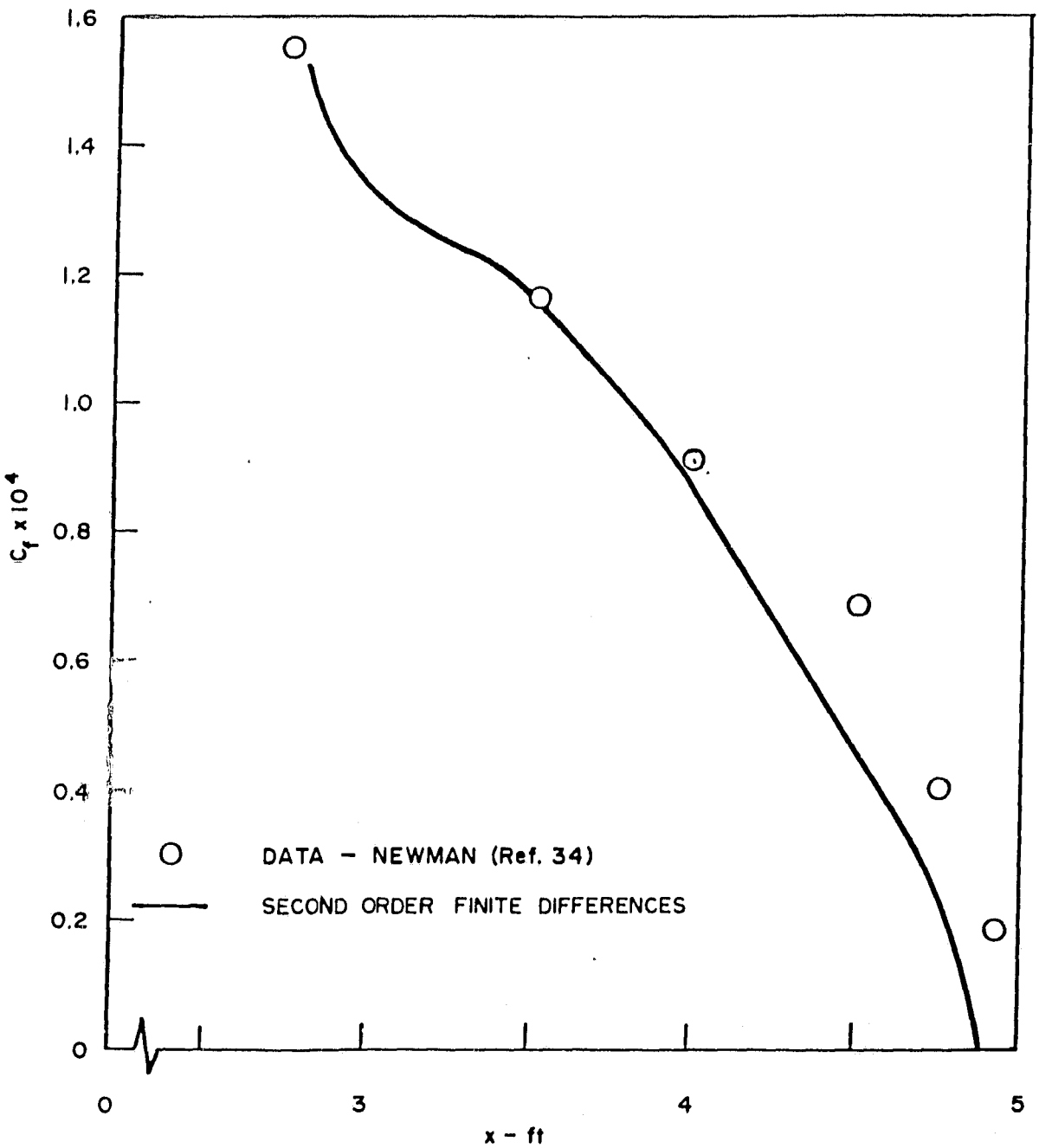

FIG. 3. NEWMAN AIRFOIL SERIES 2. SKIN FRICTION DISTRIBUTION AS A FUNCTION OF x

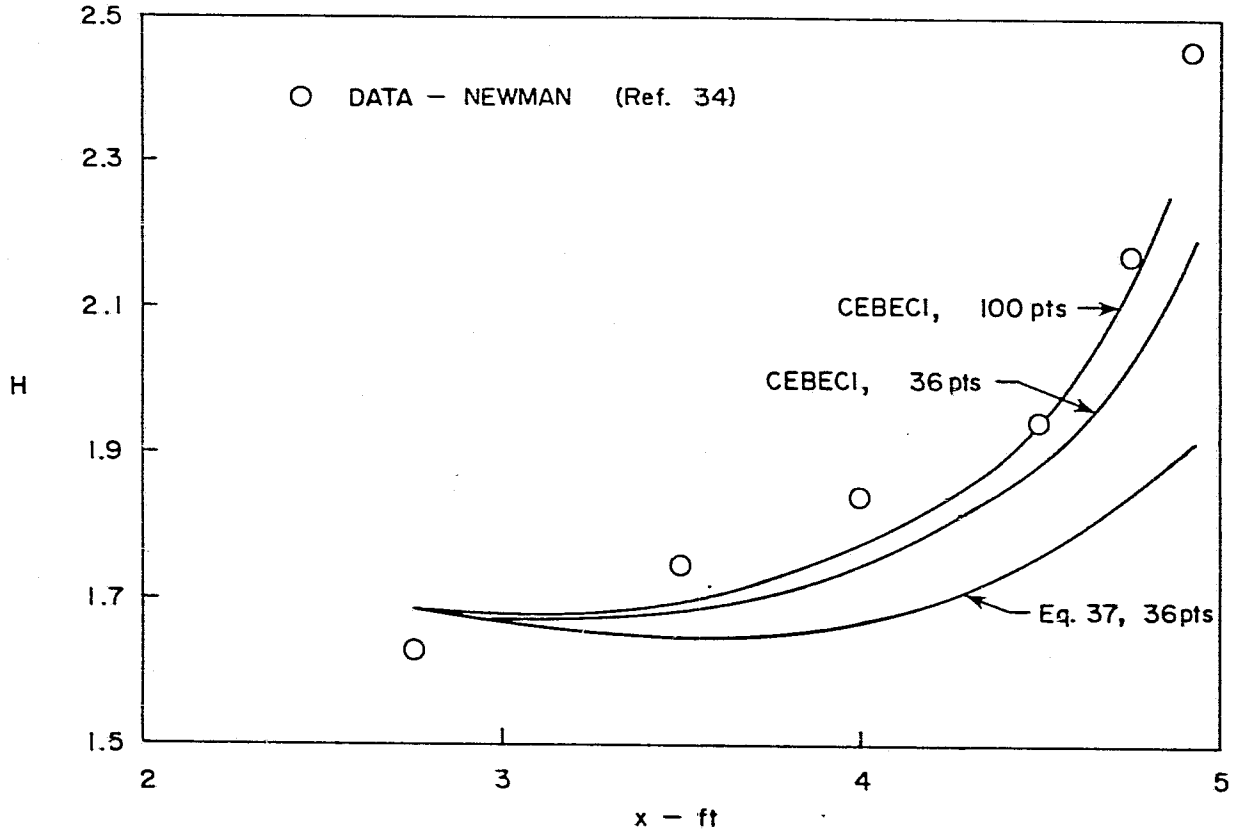

FIG. 4. COMPARISON OF SHAPE FACTOR DISTRIBUTION

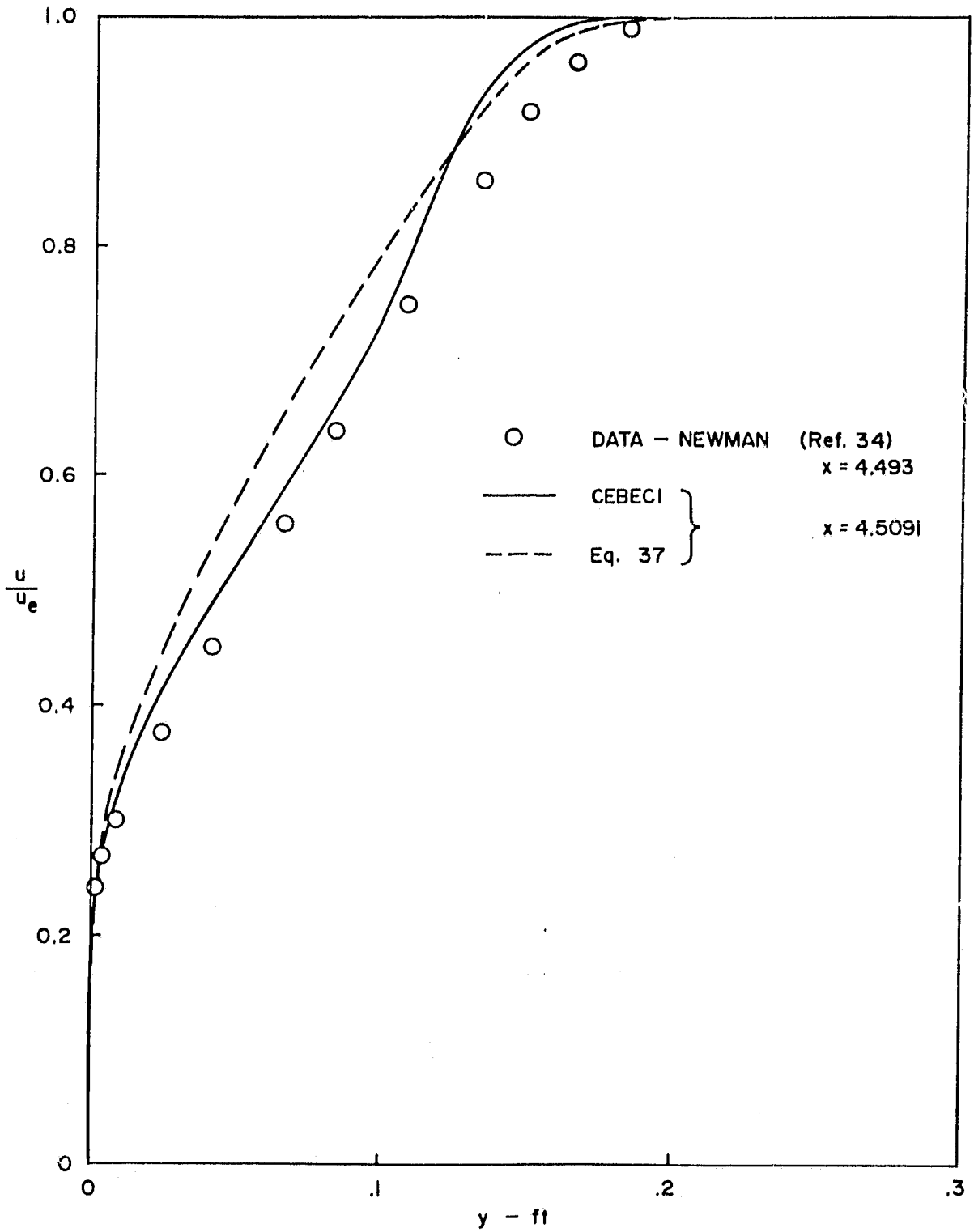

FIG. 5. COMPARISON OF VELOCITY PROFILES

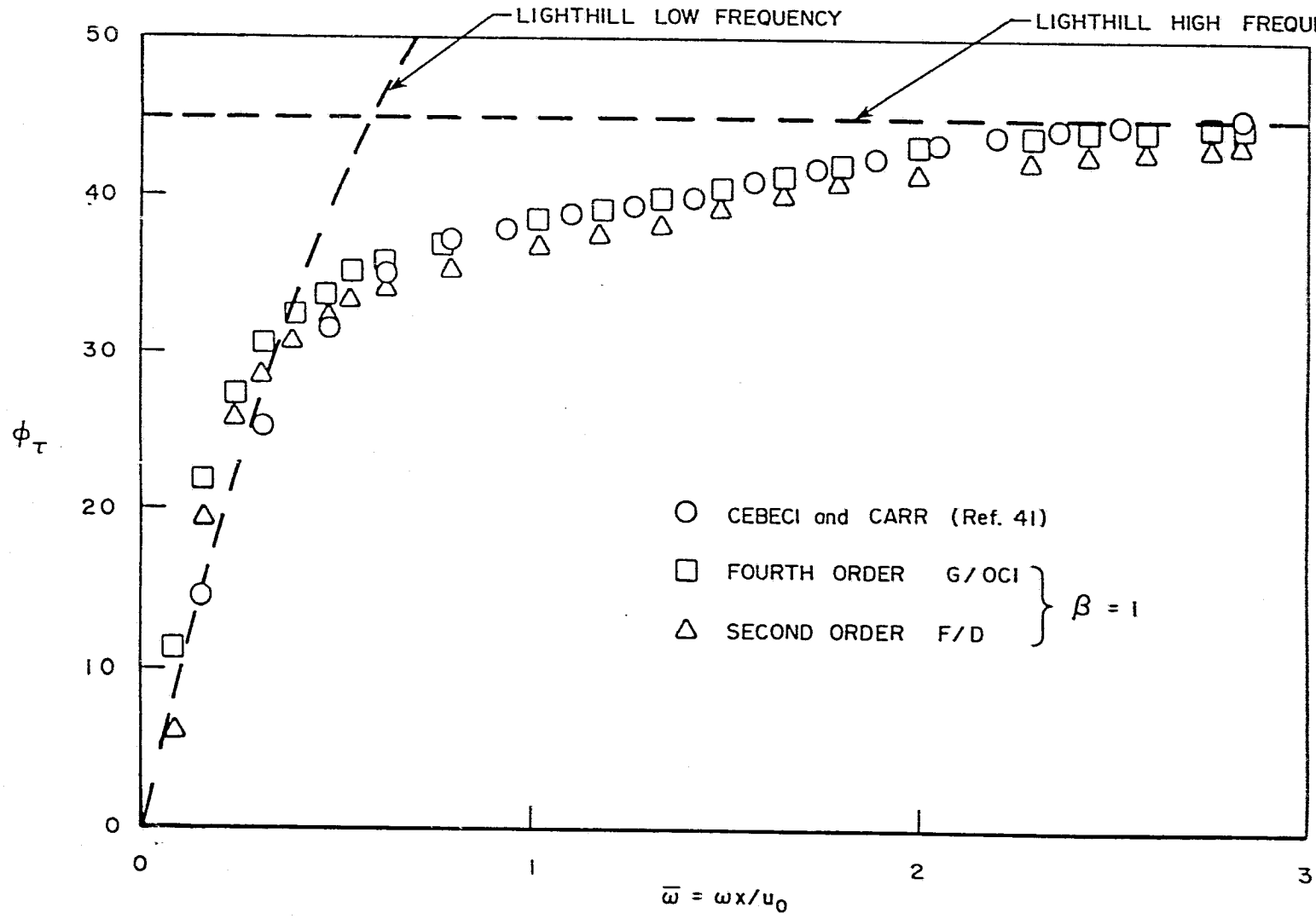

FIG. 6. PHASE ANGLE BETWEEN EDGE VELOCITY AND WALL SHEAR STRESS AS A FUNCTION OF REDUCED FREQUENCY

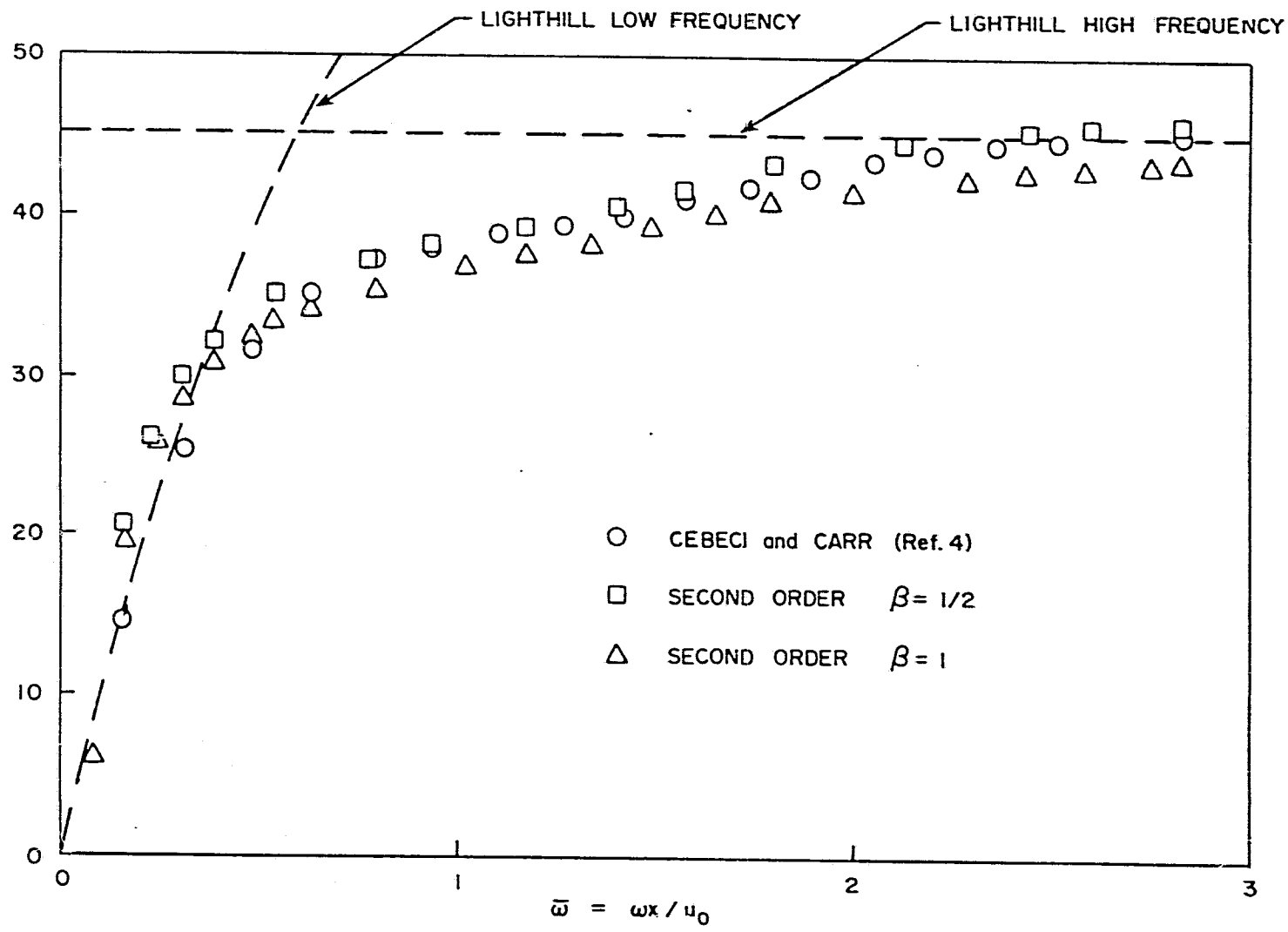

FIG. 7. PHASE ANGLE BETWEEN EDGE VELOCITY AND WALL SHEAR STRESS AS A FUNCTION OF REDUCED FREQUENCY